Deanship of Graduate Studies
Al-Quds University

Pure exciton-magnon sidebands in optical transition of manganese compounds

Shadia Yousif Mohammad Al-Tel

M.Sc. Thesis

Jerusalem-Palestine

1427 / 2006

Pure exciton-magnon sidebands in optical transition of manganese compounds

Prepared by:
Shadia Yousif Mohammad Al-Tel

B. Sc. In physics from Al-Quds University, Palestine

Supervisor: Dr. Saker Darwish

Thesis Submitted in Partial Fulfillment of Requirements for the Degree of Master of Science, Department of Physics / College of Science and Technology / Al-Quds University

1427 / 2006

Al-Quds University
Deanship of Graduate Studies
Program of Graduate Studies / Physics Department

.....

Pure exciton-magnon sidebands in optical transition of manganese compounds

Prepared By: **Shadia Yousif Mohammad Al-Tel**
Registration No. 20311981

Supervisor: Dr. Saker Darwish

Master thesis submitted and accepted, Date: 3/6/2006

Committee Members	**Signature**
Wael Kareen, Ph. D. (External Examiner)	
Abdelkarim Saleh, Ph. D. (Internal Examiner)	
Saker Darwish, Ph. D. (Chairman)	

Jerusalem-Palestine

1427 (Hijri) / 2006 (A.D.)

بسم الله الرحمن الرحيم

"و فوق كل ذي علم عليم"

صدق الله العظيم

(يوسف 76)

DECLARATION

I certify that this thesis, which is submitted for the degree of master, is the result of my own research, except where otherwise acknowledged, and that this thesis (or any part of the same) has not been submitted for a higher degree to any university or institution.

Signed..Shadia.....

Shadia Yousif Mohammad Al-Tel

3/6/2006

Acknowledgments

I would like to express my profound gratitude to my research advisor Dr. Saker Darwish for his guidance, valuable discussion, and continuous support through all stages of this work. My thanks will be extended to faculty and staff members of the physics department for their help and support during my graduate work. My thanks to committee members: Dr. Wael Kareen (External Examiner) and Dr. Abdelkarim Saleh (Internal Examiner). Special thanks to my family and friends for their support and encouragement.

Dedication

To My Parents.....

With Love.....

Abstract

Several transition bands in the visible and ultraviolet range appear in the absorption spectra of manganese compounds. One of these transitions is $^6A_{1g}(^6S) \rightarrow {}^4A_{1g}, {}^4E_g(^4G)$ corresponding to the C-band in antiferromagnetic MnF_2 compound. The complex structure for the C-band appears below the Neel temperature (T_N = 67.3 K), where the spins of manganese ions are ordered antiferromagnetically. At 10 K the C-band showed a highly complex structure with several transition lines.

In addition to the vibronic interaction, the exchange interaction helps to break down both the parity and the spin selection rules for most of the exciton-magnon transitions. The negligible temperature dependence of the line position and intensity of the C-band in the paramagnetic region is an indication of this an exciton-magnon absorption band.

The fine structure of the C-band is produced as a result of the exchange interaction between the neighboring manganese ions in the magnetic crystal. The analysis of the fine structure of the C-band yields four groups of these transition lines. Each group contains three lines. One of the lines showed prominence at different temperature ranges. These prominent peaks satisfy the spin selection rule and showed different behavior from the other peaks with rising temperature. They are labeled as pure exciton lines. The two sidebands associated with each exciton line came as a result of the exchange interaction between neighboring manganese ions and are labeled as cold and hot sidebands in reference to higher and lower energy with respect to the exciton line.

Theoretical calculation of the energy differences between the peak lines of the C-band are determined by using the spin-spin coupling. The theoretical interpretation fits well with the experimental data in terms of the number of lines, the energy separation between the lines, and the behavior of these transitions with rising temperature.

الملخص

طيات انتقالية متعددة في نطاق الضوء المرئي وفوق البنفسجي تظهر في الطيف الممتص لمركبات المنغنيز. احدى هذه الانتقالات تحدث بين المستوى $^6A_{1g}(^6S)$ و المستوى $^4A_{1g}(^4G)$، $^4E_g(^4G)$ الذي يقابل C-band في مركب فلوريد المنغنيز غير الممغنط. التركيب المعقد في C-band يظهر تحت حرارة نيل (حرارة نيل بلورة فلوريد المنغنيز تعادل 67.3 كلفن) حيث العزوم المغزلية لايونات المنغنيز تترتب بشكل متعاكس (Antiferromagnetically). كما وان التركيب المعقد في C-band يظهر عدة خطوط انتقال عند درجة 10 كلفن.

إضافة إلى الية الاهتزازهناك الية التفاعل المتبادل التي تساعد بشكل كبير في تفكيك كل من قاعدتي الازدواجية وانتقاء العزم المغزلي في معظم انتقالات exciton-magnon، باهمال الاعتماد القليل لموقع وشدة C-band على درجة الحرارة في المجال البارامغناطيسي يشير الى أن هذه الطية هي عبارة عن امتصاص exciton-magnon.

التركيب الدقيق في C-band ظهر نتيجة الية التفاعل المتبادل بين ذرات المنغنيز المتجاورة في البلورة. أظهرت نتائج التحليل للتركيب الدقيق في C-band أربع مجموعات من خطوط الانتقال. كل مجموعة تحتوي على ثلاثة خطوط، احدى هذه الخطوط تبقى ظاهرة عند درجات حرارة مختلفة. الخطوط الرئيسية في المجموعات الاربع تحقق قاعدة العزوم المغزلية المنتقاة وتظهر سلوكا مختلفا عن الخطوط الاخرى بزيادة درجة الحرارة وتسمى (Exciton lines). الطيات الجانبية المرافقة لكل خط exciton تظهر كنتيجة للتفاعل المتبادل بين ذرات المنغنيز المتجاورة وتسمى الطيات الجانبية الباردة والساخنة. الطيات الباردة تكون ذات طاقة اكبر من طاقة خط exciton في حين ان الطية الساخنة ذات طاقة اقل من طاقة خط exciton .

الحسابات النظرية لفروقات الطاقة بين قمم الخطوط في C-band وجدت باستخدام الية الممازجة بين عزمين مغزليين. التفسير النظري تطابق بشكل جيد مع القيم العملية في ما يتعلق بعدد الخطوط وفروقات الطاقة بينها ومسلك تلك الانتقالات بزيادة درجة الحرارة.

Table of Contents

Figure Captions

List of Tables:

List of Appendices:

Chapter One

Introduction

1.1 Introduction

MnF_2 is a well-known Antiferromagnet with Neel temperature T_N=67.3 K as reported by Heller and Benedek (1962), Ferguson, Guggenheim, and Tanabe (1966). Antiferromagnetism means spins are ordered in an anti parallel arrangement with zero moment at temperatures below Neel temperature (Kittle, 1996).

Experimental investigation for manganese compounds revealed several optical absorption bands in the visible and near ultraviolet regions due to partially allowed electric dipole transitions which are attributable to d^5-d^5 transitions of Mn^{+2}. These bands labeled as A, B, C, D, E... corresponding to the transitions from $^6A_{1g}(^4S)$ to $^4T_{1g}(^4G)$, $^4T_{2g}(^4G)$, $^4E_g(^4G)$, $^4A_{1g}(^4G)$, $^4T_{2g}(^4D)$, and $^4E_g(^4D)$… respectively.

These electric dipole transitions are forbidden by parity and spin selection rules. Several mechanisms which break down the selection rules must be considered. The parity selection rule can be broken down by phonon perturbation (vibronic interaction) which causes the mixing of odd-parity wave function into the even-parity electronic wave function. The spin selection rule can be broken down by the exchange interaction resulting from the spin-spin interaction between neighboring ions in magnetic crystal. Detailed discussions of these mechanisms will be presented in latter chapters.

Recently the study of optical properties of magnetic compounds has developed rapidly from both the theoretical and the experimental sides. Most of the experimental works have concentrated on the temperature dependence of these optical transitions. It is important to understand the nature of these transitions labeled as magnon sidebands (exciton-magnon band).

1.2 Review of optical transitions studies in manganese compounds.

The electronic absorption spectrum of Mn^{+2} has been the subject of many studies for a long time. In this section, I will briefly present some of these studies and their major results of interest: Ferguson (1968) reported the electronic absorption spectra of $KMnF_3$, $RbMnF_3$ and MnF_2. Tsujikawa and Kanda (1963), Lawson (1966), and Goode (1965) investigated the optical transitions for different manganese compounds, particularly in relation to the effects of exchange interaction.

The first observation of magnon sidebands in MnF_2 was made by Green, Sell, Yen, and Schawlow (1965). The more detailed results of this transition have been reported by Sell (1968). These studies showed that the magnon sideband arises from the creation of an exciton and the simultaneous creation or annihilation of magnons. Absorption spectra of $CsMnF_3$ in the 3900 Å region were investigated by Saito (1970), where he classified hyperfine structures into three categories: Exciton lines, Magnon-sidebands and Phonon-sidebands

Several studies (for example Sell, Green, and White, 1967; Sell, 1968; Moriya and Inoue, 1968; and Eremenko, 1977) indicated that the magnon sideband involved one or more magnons in different manganese compound. Motizuki and Harada (1970) explained the temperature dependence of the optical absorption in MnO and MnS in the range of transitions $^6A_{1g} \rightarrow {}^4T_{1g}$ and $^6A_{1g} \rightarrow {}^4T_{2g}$ of Mn^{+2} ion in terms of sidebands associated with magnons. Tanaka (1971) obtained the thermal behavior of the magnon sidebands for MnF_2 in the whole temperature region using the Green's function method.

The study of Harada and Motizuki (1972) showed that there are two kinds of magnon sidebands: one is labeled as cold sideband, and the other is hot sideband depending on their energy and intensity relative to the original line. The cold band appears when the absorption corresponding to the creation of magnons and that corresponding to the annihilation of magnons is the hot band. Tanabe and his collaborators (Fujiwara, Gebhardt, Petanides, and Tanabe, 1972, Shinagawa and Tanabe, 1971, and Fujiwara and Tanabe, 1971) have derived the general theoretical formula for the temperature dependences of the intensity, peak position, and half-width of the magnon sidebands in MnF_2 and $RbMnF_3$.

Yen, Imbusch, and Huber (1967) reported the temperature dependence of the peak position and half-width of the cold sideband observed in MnF_2 and compared their results with magnetic energy. Seehra and Abumansoor (1985) discussed the effect of antiferromagnetic ordering on the two optical absorption bands (C and F) in MnF_2, where they found that there is a blue-shift noticeable of these bands agrees with the change of the sublattice magnetization below T_N.

Tsuboi and Ahmet (1992) studied the temperature dependence of the exciton and magnon sideband absorption in MnF_2 crystal, and they found a good agreement of their experimental data with the Shinagawa and Tanabe's theoretical calculation for each intensity of the cold and hot magnon sidebands.

Few papers discussed the fine structure of some bands in different manganese compounds. Yokogawa, Taniguchi, and Hamaguchi (1977) observed the fine structure of A, C, and D bands interpretated in MnO bellow 10 K, based on the combination of the three kinds of excitation (exciton-exciton, exciton-magnon, and exciton-magnon-phonon). Also Moncorge and Jacquier (1981) observed the fine structure of pure exciton and magnon side band in $^4T_{1g}$ (^4G) excited state of Mn^{+2} ions in antiferromagnet $BaMnF_4$.

Raman spectroscopy was employed to study the spin-spin interaction in MnF_2 and FeF_2 by many groups (for example: Suzuki and Kamimura, 1973; Lockwood, Katiyar, and V. C. Y. So, 1983; Lockwood and Cottam, 1988). These studies showed that the Raman frequencies, line width, and integrated intensity of magnetic compounds are affected by the exchange coupling between magnetic ions.

The shape of the spectra of different antiferromagnetic manganese compounds in the different ranges of transitions had been studied by Malakhovskii, Filimonov, and Goncharov (1989), Eremenko and Shapiro (1990), and Eremenko, Kachur, Piryatinskaya, Shapiro (1994). Such studies showed the optical transitions in antiferromagnetic crystal involving the spin-wave subsystem (exciton-magnon transitions).

The temperature dependence of both bands C-band ($^6A_{1g}\rightarrow{}^4A_{1g}$, ^4E_g (^4G)) and E-band ($^6A_{1g}\rightarrow{}^4E_g$ (^4D)) in $RbMnF_3$ absorption spectra above T_N have been studied by Malakhovskii, Vasilev, and Morozova (1986). They found that the spectra of both transitions are caused by excitation of a number of quanta of odd vibrations.

The temperature dependence of oscillator strength and the line position E from 10 K to 300 K of the two exciton bands α (A+A) and β (A+B) in MnF_2 and $RbMnF_3$ were discussed by Darwish, Abumansoor, and Seehra (1986). The thermal behavior of the two exciton bands α (A+A) and γ (A+C) and the vibronically induced bands in $KMnF_3$ and $RbMnF_3$ were presented by Darwish and Seehra (1988).

Hoekstra and Hass (1985) reported the optical absorption of $MnCl_2$ in the spectral region 16000-30000 cm^{-1} at temperatures between 2.7 and 250 K. In this study it is found that the exchange interaction mechanism plays an important role to overcome the parity and the spin selection rules to allow the d-d transitions.

Popov and Edelman (2003) studied the external magnetic field, the temperature and the uniaxial pressure effects on the fine structure of the transition $^6A_{1g}\rightarrow{}^4T_{2g}$ (^4D) (D-band) in $RbMnCl_4$. This study indicated that there are exciton-magnon, exciton-phonon, and other multi particle excitations in this optical spectrum.

Popov and Ovchinnikov (2003) investigated the magnon satellite bands in the optical absorption spectrum in antiferromagnetic Rb_2MnCl_4 in the range of transition $^6A_{1g}(^4S) \rightarrow {}^4A_{1g}$, ^4E_g (^4G). This study revealed that there are two magnon satellites (hot and cold) of the exciton-magnon bands in this absorption.

The focus of my work is to explain the fine structure of the pure exciton-magnon sideband in the optical spectrum for MnF_2 compound in the range of transition $^6A_{1g}(^6S) \rightarrow {}^4A_{1g}$, $^4E_g(^4G)$ correspond to the C-band at low temperature. To achieve my objectives, the subsequent chapters of the thesis are arranged as follows: In chapter II a theoretical background and brief discussion of the crystal structure of MnF_2, crystal field theory, octahedral field, electromagnetic radiation, selection rules, vibronic interaction and exchange interaction. Chapter three presents a review of experimental data. Chapter four contains analysis and discussion of the experimental data. Chapter five is a summary of the major results in my work.

Chapter Two

Theoretical Considerations

The crystal structure of MnF_2 compound is shown in figure 2.1, with Mn^{+2} ion considered as the central ion of the system surrounded by several equivalent electrons. This structure presents a theoretical challenge to solve for the possible energy levels for Mn^{+2}. The energy levels of Mn^{+2} in MnF_2 crystal depends on several factors, we need to know how the central ion is affected by crystalline field. In addition, we need to review several important topics, which are briefly presented in this chapter and divided into nine sections. Starting with crystal structure to MnF_2, crystal field theory, a review of the five d-orbitals and how these orbitals affected by octahedral field, the energy level of Mn^{+2}, the interaction of radiation with matter, and the selection rules. In the final two sections, a discussion of the vibronic interaction and exchange interaction will be presented.

2.1 Crystal structure of MnF_2

MnF_2 crystal has a rutile-type structure belonging to the space group $P4_2/mnm$ with lattice constants a=4.8734 Å and c=3.3099 Å at room temperature (Wyckoff, 1948, Griffel and Stout, 1950). The manganese ions occupy the corners and the center of the unit cell forming a body centered tetragonal lattice as shown in figure 2.1.
Below T_N (=67.3 K), the spins of manganese ions are ordered antiferromagnetically along the z-axis, where the body-center ions of the unit cell form the up-spin sublattice, and the corner ions form the down spin sublattice (Erickson, 1953). The manganese ions of the unit cell coupled with exchange parameters J, J', and J" shown in figure 2.1 were estimated to be respectively 1.225 cm^{-1} (Trapp and Stout, 1963), and -0.22 cm^{-1}, and -0.035 cm^{-1} (Okazaki, Tuberfield, and Stevenson, 1964).

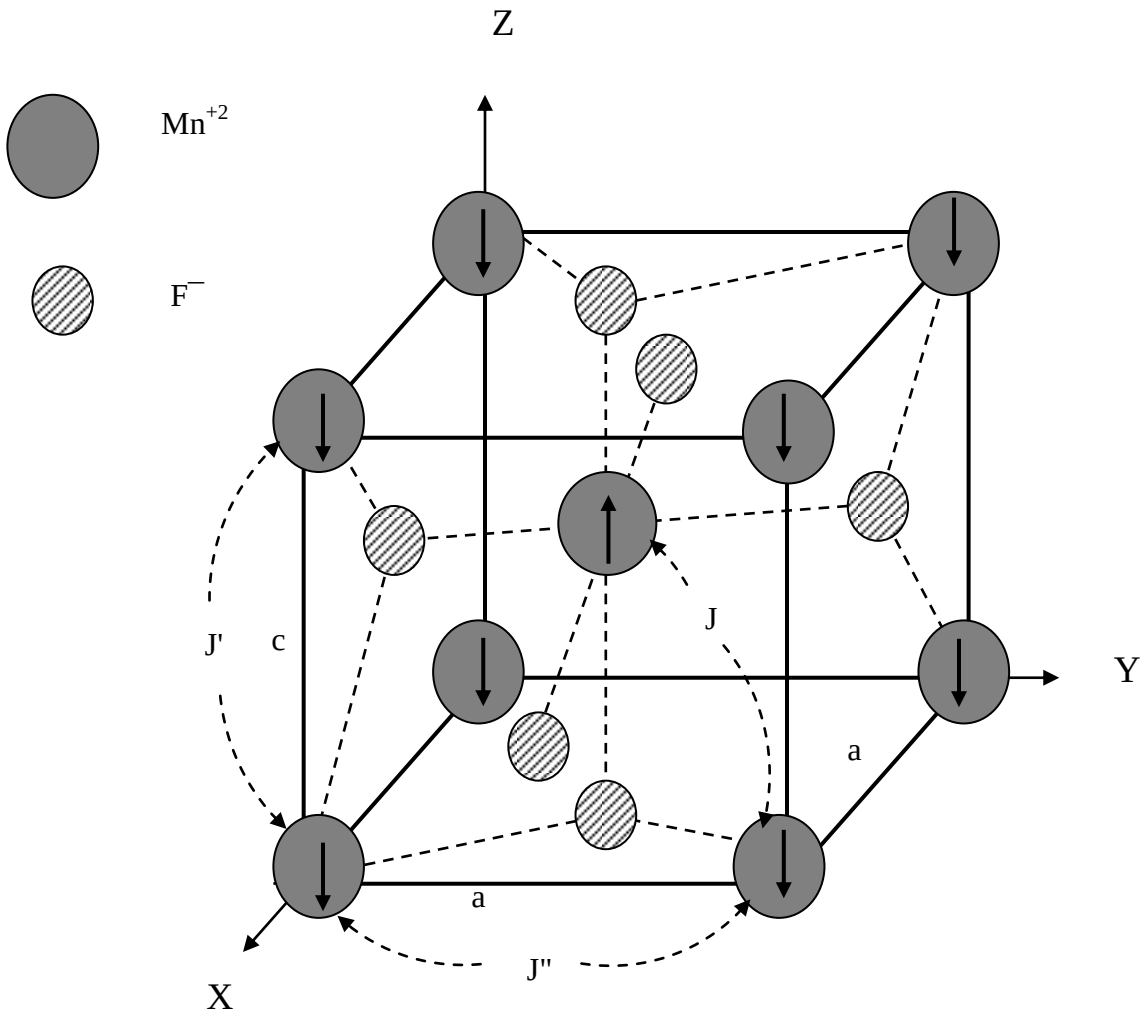

Figure 2.1: MnF_2 crystal structure.

2.2 Crystal field theory

Crystal field is produced when a metal ion is located in a little cavity inside a crystalline lattice, and is exposed to the electric field from the surrounding atoms or molecules called ligands. Bethe was the first to develop the idea of a ligand field in 1929.
In the case of MnF_2, Mn^{+2} is the central ion surrounded by six negative charges located on the vertices of an octahedron as shown in Fig.2.2. These negative charges induce an effect on Mn^{+2} giving the total electrostatic potential which destroys the spherical symmetry of this ion.

Several studies for the crystal field theory had been carried through with elaborate details as in Ballhausen (1962), Low (1960), Figgis (1966), Sugano, Tanabe, and Kamimura (1970), and Figgis and Hitchman (2000).

The Hamiltonian for the central ion includes two terms: V_c due to the ligands and H_f for the free ion (Ballhausen, 1962):

$$H = H_f + V_c \tag{2.1}$$

The total Hamiltonian can be written as:

$$H = -\frac{\hbar^2}{2m}\sum_i \nabla_i^2 - \sum_i \frac{ze^2}{r_i} + \frac{1}{2}\sum_{i\neq j}\frac{e^2}{r_{ij}} + \sum_i \xi(r_i)\vec{l}_i.\vec{s}_i + V_c \tag{2.2}$$

The first four terms make up the Hamiltonian for the free ion, in the following order: The first term is the kinetic energy for the i^{th} electron, the second term is the coulomb potential energy of i^{th} electron in the nucleus field, the third term is the electronic repulsion between i^{th} electron and j^{th} electron, and the fourth term is due to the spin-orbit coupling.

Depending on the relative strength of the V_c with respect to the electronic repulsion perturbing term there will be three cases (Low, 1960, Henderson and Bartram, 2000):

$$V_c < \sum e^2 / r_{ij} \qquad \text{Weak crystal field (high spin arrangement).}$$

$$V_c \cong \sum e^2 / r_{ij} \qquad \text{Medium crystal field.} \tag{2.3}$$

$$V_c > \sum e^2 / r_{ij} \qquad \text{Strong crystal field (low spin arrangement).}$$

The reason for distinguishing these three cases is to define the dominant perturbation term to a first order approximation. The strong field approximation is appropriate when the crystal

field is dominant and causes a splitting larger than the electronic repulsion (Tanabe and Sugano, 1954). In the weak field approximation, the crystal field perturbation is small compared to the electronic repulsion effect. The electronic repulsion effect on energy levels of the ion comes first, and crystal field effect comes second. In both cases weak and strong fields, the spin-orbit coupling is a small term and is treated as a perturbation. The medium field case appears when both the crystal field and electronic repulsion are approximately the same order of magnitude (Ballhausen, 1962, Griffith 1961, and Figgis and Hitchman (2000).

To determine the ground state for the manganese ion, we apply Hund's rules: The term with the highest multiplicity (high spin arrangement) is lowest in energy; If there is more than one term with the highest multiplicity, then the term with the highest multiplicity and largest value of L lies lowest (Levine, 1983). In addition we must stay consistent with the Pauli exclusion principle (No two electrons in the same atom can have the same values of all four quantum numbers n, l, m_l, and m_s)(Slater, 1960). Therefore, the ground state for Mn^{+2} of d^5-configuration is $^6S_{5/2}$ and the weak field approximation is necessary to set up in our case.

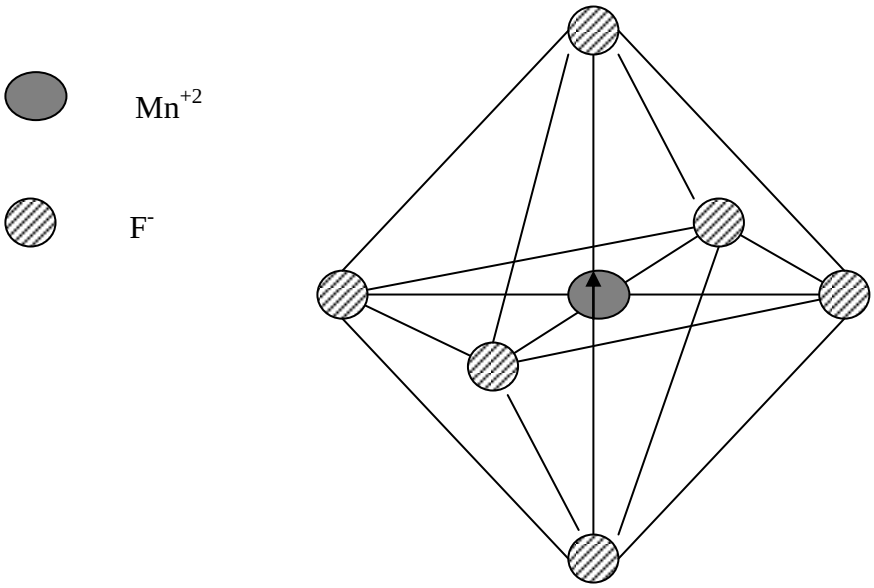

Figure 2.2: Crystal field model of the octahedral complex.

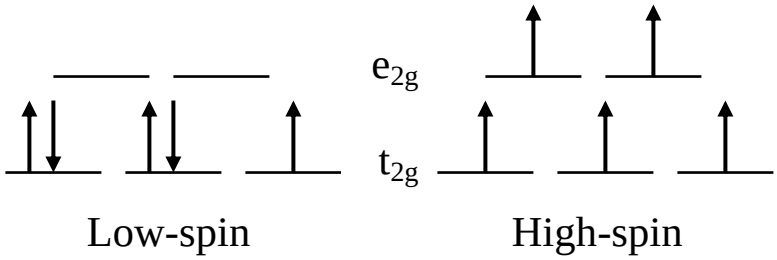

Figure 2.3: Low and high spin arrangement of five d-electrons after Huheey, E. Keiter, and R. Keiter (1993)

2.3 The Five d-orbitals:

The wave function of a single electron is given by (Griffiths, 1995):

$$\psi_{n,l,m_l} = R_{nl}(r) Y_l^{m_l}(\theta,\phi) \qquad 2.4$$

where $R(r)$ is the radial part, and $Y(\theta,\phi)$ is the spherical harmonics part containing $\Theta(\theta)$ and $\Phi(\phi)$. The numbers n, l, m_l are the quantum numbers (n is the principle quantum number, l is an orbital angular momentum number, and m_l is the z-component of the orbital angular momentum, running from l to $-l$.

Usually, a single d-electron in a free ion has a wave-function that belongs to a five fold degenerate set corresponding to the five values of m_l.
The five d- orbitals are specified by spherical harmonics as follows (Ballhausen, 1962):

$$Y_2^{\,0} = (5/8)^{1/2}\left(3\cos^2\theta - 1\right).(2\pi)^{-1/2}$$

$$Y_2^{\pm 1} = (15/4)^{1/2}\sin\theta\cos\theta.(2\pi)^{-1/2}\, e^{\pm i\phi} \qquad 2.5$$

$$Y_2^{\pm 2} = (15/16)^{1/2}\sin^2\theta\,.(2\pi)^{-1/2}\, e^{\pm 2i\phi}$$

By making suitable combinations of the above wave functions, which are described in appendix A, the five d wave functions in their real forms are:

$$d_{z^2} = [(0)] = \frac{1}{2}\left(3z^2 - r^2\right)$$

$$d_{x^2-y^2} = 2^{-\frac{1}{2}}[(2)+(-2)] = \frac{\sqrt{3}}{2}\left(x^2 - y^2\right)$$

$$d_{xy} = 2^{-\frac{1}{2}}[(2)-(-2)] = \sqrt{3}(xy) \qquad 2.6$$

$$d_{yz} = 2^{-\frac{1}{2}}[(1)-(-1)] = \sqrt{3}(yz)$$

$$d_{xz} = 2^{-\frac{1}{2}}[(1)+(-1)] = \sqrt{3}(xz)$$

where (0), (2), (-2)… indicate wave functions corresponding to m_l = 0, 2, -2...

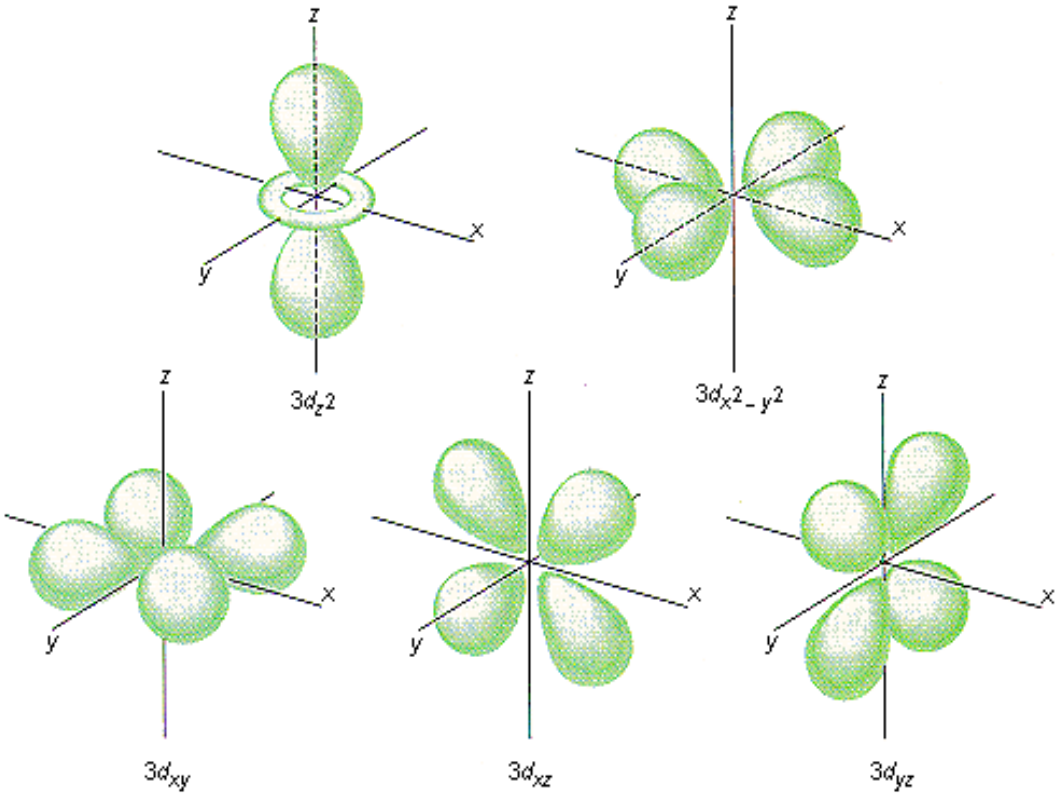

Figure 2.4: The real angular part of five d-orbitals wave function after Cotton and Wilkinson (1980).

2.4 Manganese ion energy levels

Manganese ion (Mn^{+2}) has a configuration $1S^2 2S^2 2P^6 3S^2 3P^6 3d^5$. It is considered as one of transition-metal ions that are characterized with open nd shells, where the principle quantum number n equals three. There are five electrons in d-orbitals corresponding to different values of m_l and m_s (m_l is the z-component of orbital angular momentum l, which has several values from $-l \ldots\ldots +l$, and m_s is the z-component of spin angular momentum s, which has several values from $-s \ldots\ldots +s$) (Liboff, 1992). According to Hund's rules, the ground state in Mn^{+2} is $^6S_{5/2}$ where the five electrons in the d-orbital have spins up.

The other possible ways of configuration for these electrons in d-orbital forms are the possible excited states ^4G, ^4F, ^4D...etc. These differ for different values of M_L and M_S, where M_L is the z-component of the total orbital angular momentum L, and M_S (multiplicity of a state) is the z-component of the total spin angular momentum S.

The total orbital angular momentum (L) that arises from two electrons runs from $|l_1 - l_2| \ldots |l_1 + l_2|$, and the total spin angular momentum (S) runs from $|s_1 - s_2| \ldots |s_1 + s_2|$. $M_L = \sum_i m_{l_i} = 2L + 1.$, and $M_S = \sum_i m_{s_i} = 2S + 1$ (Eisberg and Resnick, 1974).

For the ($3d^5$) configuration, the five electrons in d-orbitals have the same quantum numbers n, l, and s but different values of m_l and m_s.

n = 3

$l_1 = l_2 = l_3 = l_4 = l_5 = 2$

$s_1 = s_2 = s_3 = s_4 = s_5 = 1/2$.

The minimum value of L is 2 and the maximum value is 10, so the possible values of L are 2, 3, 4, 5, 6, 7, 8, 9, and 10. The possible values of S for the same configuration are 1/2, 3/2, and 5/2.

The possible states for d^5 configurations are expressed in terms of L and S with the following nomenclature:

$$^{2S+1}\mathrm{L} \qquad 2.7$$

where L = S P D F..., and (2S+1) is the multiplicity of the term. The degeneracy of any term is (2L + 1) (2S + 1). Each value of M_L occurs (2S + 1)-times, and each value of M_S occurs (2L + 1)-times. For example a ^3P state has nine- fold degenerate (Figgis, 1966).

By applying, the above rules and the exclusion principle, the possible states for Mn^{+2} are (Levine, 1983):

$^6S,\ ^4G,\ ^4F,\ ^4D,\ ^4P,\ ^2I,\ ^2H,\ ^2G(2),\ ^2F(2),\ ^2D(3),\ ^2P,\ ^2S$

Some examples for excited states of the d^5 configurations

d^5 - configuration	M_L	M_S	ground term	degeneracy
m_l = 2 1 0 -1 -2				
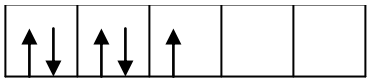	6	1/2	^{2}I	26
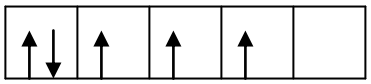	4	3/2	^{4}G	36
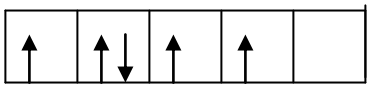	3	3/2	^{4}D	28

All of the above terms split by spin-orbit coupling into states which are specified by the total angular momentum J, that ranges from | L - S | to | L + S |. To specify a particular state, the value of J is added as a subscript to the term symbol, and then the full symbol for a state is given by (Slater, 1960):

$$^{2S+1}L_J \qquad 2.8$$

The coulomb interaction between electrons in d-orbitals is characterized by the so called electron repulsion parameters. These parameters are classified using two completely equivalent ways: either in Racah parameters, A, B, and C (Racah, 1942) or in Condon and Shortley parameters F_0, F_2, and F_4 (Condon and Shortley, 1957). The relations between the two sets are:

$$\begin{aligned} A &= F_0 - 49F_4. \\ B &= F_2 - 5\,F_4. \\ C &= 35\,F_4. \end{aligned} \qquad 2.9$$

The values of F_2 and F_4 are explained in Appendix B.

All the energy levels within each d^5 configuration having the same dependence on A and listed in table 2.1. The values of B and C are known from the fitting of spectroscopic data, where B = 960 cm^{-1} and C = 3325 cm^{-1} for Mn^{+2} (Griffith, 1961).

Table 2.1: Term energies of d^5-configuration by using Racah parameters and Condon and Shortley parameters (Laporte, 1942).

Energy in	**Racah parameters**	**Condon and Shortley parameters**
E (^{2}S)	10A – 3B + 8C	$10F_0 – 3F_2 – 195F_4$
E (^{6}S)	10A – 35B	$10F_0 – 35F_2 – 315F_4$
E (^{2}P)	10A + 20B + 10C	$10F_0 – 20F_2 – 240F_4$
E (^{4}P)	10A – 28 B + 7C	$10F_0 – 28F_2 – 105F_4$
E (^{2}D)	$10A–3B+11C \pm 3 (57B^2+2BC+C^2)^{1/2}$	$10F_0–3F_2–90F_4 \pm (513F_2^2 - 4500F_2F_4+20{,}700F_4^2)^{1/2}$
E (^{2}D$'$)	10A – 4B + 10C	$10F_0 – 4F_2 – 12F_4$
E (^{4}D)	10A – 18B + 5C	$10F_0 – 18F_2 – 225F_4$
E (^{2}F)	10A – 9B + 8C	$10F_0 – 9F_2 – 165F_4$
E (^{2}F$'$)	10A – 25B +10C	$10F_0 - 25F_2 – 15F_4$
E (^{4}F)	10A – 13B + 7C	$10F_0 – 13F_2 – 180F_4$
E (^{2}G)	10A – 13B + 8C	$10F_0 – 3F_2 – 155F_4$
E (^{2}G$'$)	10A + 3B + 10C	$10F_0 – 13F_2 – 1545F_4$
E (^{4}G)	10A – 25B + 5C	$10F_0 – 25F_2 – 190F_4$
E (^{2}H)	10A – 22B + 10C	$10F_0 – 22F_2 – 30F_4$
E (^{2}I)	10A – 24B + 8C	$10F_0 – 24F_2 – 90F_4$

2.5 Octahedral field effect on d-orbitals:

If the distribution of the charge is spherical, then all d-orbitals will be affected in the same manner and all of the d-orbitals will increase in the same amount of energy. In an octahedral arrangement, the electrons of the d-orbitals are repelled by an amount depending upon the distribution of these orbitals. The charges approach the metal ion along the Cartesian x, y, and z-axes. Thus, the orbitals along these axes (z^2, x^2-y^2) should rise in energy by a greater amount compared to the orbitals that do not lay exactly along the x, y, and z axes (xy, yz, xz). To illustrate the effect of the octahedral field on the different levels, we apply the matrix element for octahedral potential field V_{oct} on the orbital parts of a wave function of the term being considered as in the following matrix elements (Sugano, Tanabe, and Kamimura, 1970):

$$\langle M_L \mid V_{oct} \mid M'_L \rangle = \int \psi_{nlm_l} V_{oct} \psi_{n'l'm'_l} \, d\tau \qquad 2.10$$

$\psi_{nlm_l} = R_{nl}(r)\Theta_{lm_\ell}(\theta)\Phi_{m_l}(\phi)$ And the unit volume $d\tau = r^2 \sin\theta \, dr d\theta d\phi$.

$$V_c(r) = \frac{6Ze^2}{a} + V_{oct} = \frac{6Ze^2}{a} + D\left(x^2 + y^2 + z^2 - \frac{3}{5}r^4\right) \qquad 2.11$$

Where the term D is given by: $D = \frac{35ze^2}{4a^5}$ and the evaluation of V_c is presented in Appendix C.

The first term of the formula 2.11 is spherically symmetric and all the d-orbitals increase to the same value of energy without any splitting between them due to its effect. The second term splits the five d-orbitals into two levels; the following discussion explains how this splitting occurs.
The d-orbitals splitting are given in appendix D, and the non-vanishing matrix elements are:

$$\begin{aligned}
&\langle \pm 2 \mid V_{oct} \mid \pm 2 \rangle = D_q \\
&\langle \pm 1 \mid V_{oct} \mid \pm 1 \rangle = -4D_q \\
&\langle \ 0 \ \mid V_{oct} \mid 0 \ \rangle = 6D_q \\
&\langle \pm 2 \mid V_{oct} \mid \mp 2 \rangle = 5D_q
\end{aligned} \qquad 2.12$$

Here $q = \frac{2}{105}\langle r^4 \rangle_{nl}$

The secular determinant is:

$$\begin{array}{c} (2) \quad (1) \quad (0) \quad (-1) \quad (-2) \\ \begin{vmatrix} D_q - E & 0 & 0 & 0 & D_q \\ 0 & -4D_q - E & 0 & 0 & 0 \\ 0 & 0 & 6D_q - E & 0 & 0 \\ 0 & 0 & 0 & -4D_q - E & 0 \\ 5D_q & 0 & 0 & 0 & D_q - E \end{vmatrix} \end{array} = 0 \qquad 2.13$$

This can be reduced to three determinants that are readily solved to yield the energies -4Dq for a three fold-degenerate set of levels arising from the atomic orbitals of wave functions xy, yz and zx, and 6Dq for a two fold-degenerate set arising from the functions x^2-y^2 and z^2. These levels are denoted t_{2g} and e_g respectively (Sherman, 1984).
The energy splitting between them is $10D_q$.

$$\Delta E = E(e_g) - E(t_{2g}) = 6D_q + 4D_q = 10D_q$$

The five-fold degeneracy is removed in the presence of the ligand atoms and will split into two levels: A lower level (t_{2g}) by octahedral field, which is triply degenerate and upper level (e_g) is a doubly degenerate with separation energy of $10D_q$ as shown in figure 2.5.

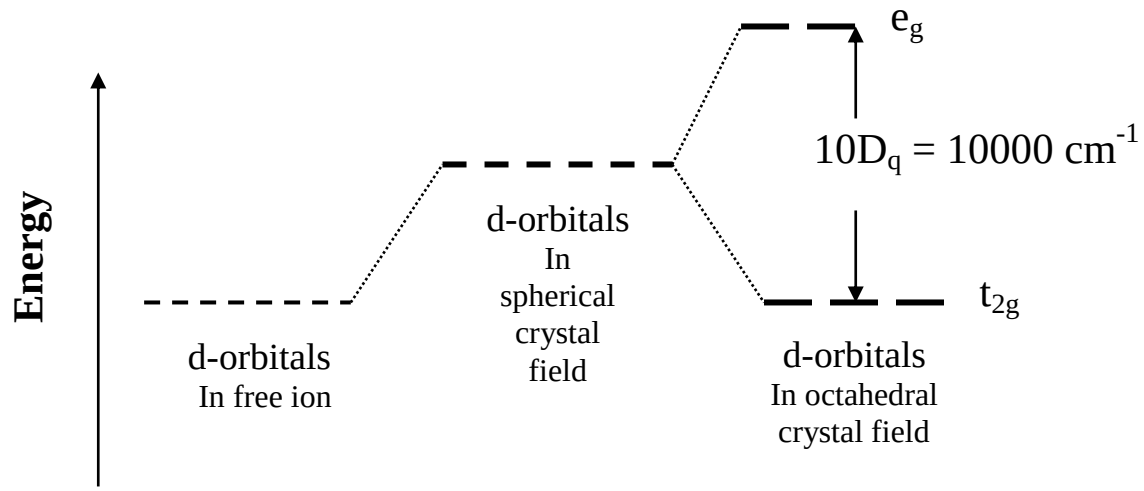

Figure 2.5: Crystal field splitting in an octahedral field

The splitting of D level the same as the splitting of the set of one electron d-orbitals. In a similar way S level and s orbital, P level and p orbitals, and so on. For the S level, it is orbitally non-degenerate, and will not be affected by the ligand field potential, and will not split (Figgis, 1966). For the P-level, each of the three p-orbitals has its maximum electron density directed at two vertices; therefore, all of the matrix elements are zero and the p-orbitals do not split by V_{oct} (Slater, 1974). The other terms have many splitting, because each of them is orbitally degenerate and the matrix element between the states of a certain level are non-zero.

For the levels F, G, H, etc, we can apply the same technique used with the S, P, and D levels wave functions. As an example, under octahedral field ^4F term splits to $^4A_{2g}+^4T_{1g}+^4T_{2g}$ with same multiplicity and ^4G term splits to $^4A_{1g}+^4E_g+^4T_{1g}+^4T_{2g}$ (g "gerade" implies the symmetry is even) which are listed in table 2.2. A common way to show these energy levels graphically and its behavior with increased D_q (D_q is a measure of crystal field theory) is shown in Orgel diagram (Orgel, 1953) in figure 2.6. Another figure presents the energy level diagrams known as Tanabe and Sugano diagram and describes how E/B changes with ratio of D_q/B. Tanabe-Sugano diagrams are more comprehensive than Orgel diagram, because they include both weak and strong crystal fields as shown in figure 2.7 for d^5 system (Yen and Selzer, 1981, Henderson and Bartram, 2000).

Table 2.2: Free ion terms in an octahedral field.

Free ion term (d^5 – configuration)	**States in octahedral field**
S	A_{1g}
P	T_{1g}
D	$E_g + T_{2g}$
F	$A_{2g} + T_{1g} + T_{2g}$
G	$A_{1g} + E_g + T_{1g} + T_{2g}$
H	$E_g + 2T_{1g} + T_{2g}$
I	$A_{1g} + A_{2g} + T_{1g} + 2T_{2g}$

The ground state in Mn^{+2} has only one state S=5/2. All of the observed main transitions occur from the ground state (sextet) to one of the excited states (quartet, singlet…), as shown in figure 2.8.

From the Orgel diagram, we noticed that some of the energy levels are shifted to higher or lower energies with increasing D_q. For example $^4T_{1g}(^4G)$, $^4T_{2g}(^4G)$, and $^4T_{2g}(^4F)$. On the other hand, $^4E_g(^4D)$, $^4A_{2g}(^4F)$, and $^4A_{1g}(^4G)$, $^4E_g(^4G)$ are unaffected by the crystal field strength, because these levels have the same configurations as the ground state ($t_{2g}^3\ e_g^2$), these levels are negligible phonon effect. The spectral lines connecting the terms of the same configuration are expected to be observed as sharp lines (Tanabe and Sugano, 1954). The excited states $^4A_{1g} + ^4E_g$ (^4G) are degenerate in the crystal field. A lifting of the degeneracy can be produced by the covalency. When we consider the distance between the ligands and the metal ion is small, the electron clouds of the metal and of the ligands overlap and some of the electrons undergo exchange between them. Therefore the metal and ligand orbitals are

admixed, resulting in the change of the electrons energies in the ligands and metal ion orbitals (Koide and Pryce, 1958). The $^4A_{1g}$, $^4E_g(^4G)$ splitting is about 143 cm^{-1} in MnF_2 due to covalency (Schwartz, Spencer, Yeakel, Schatz, and Maisch, 1974).

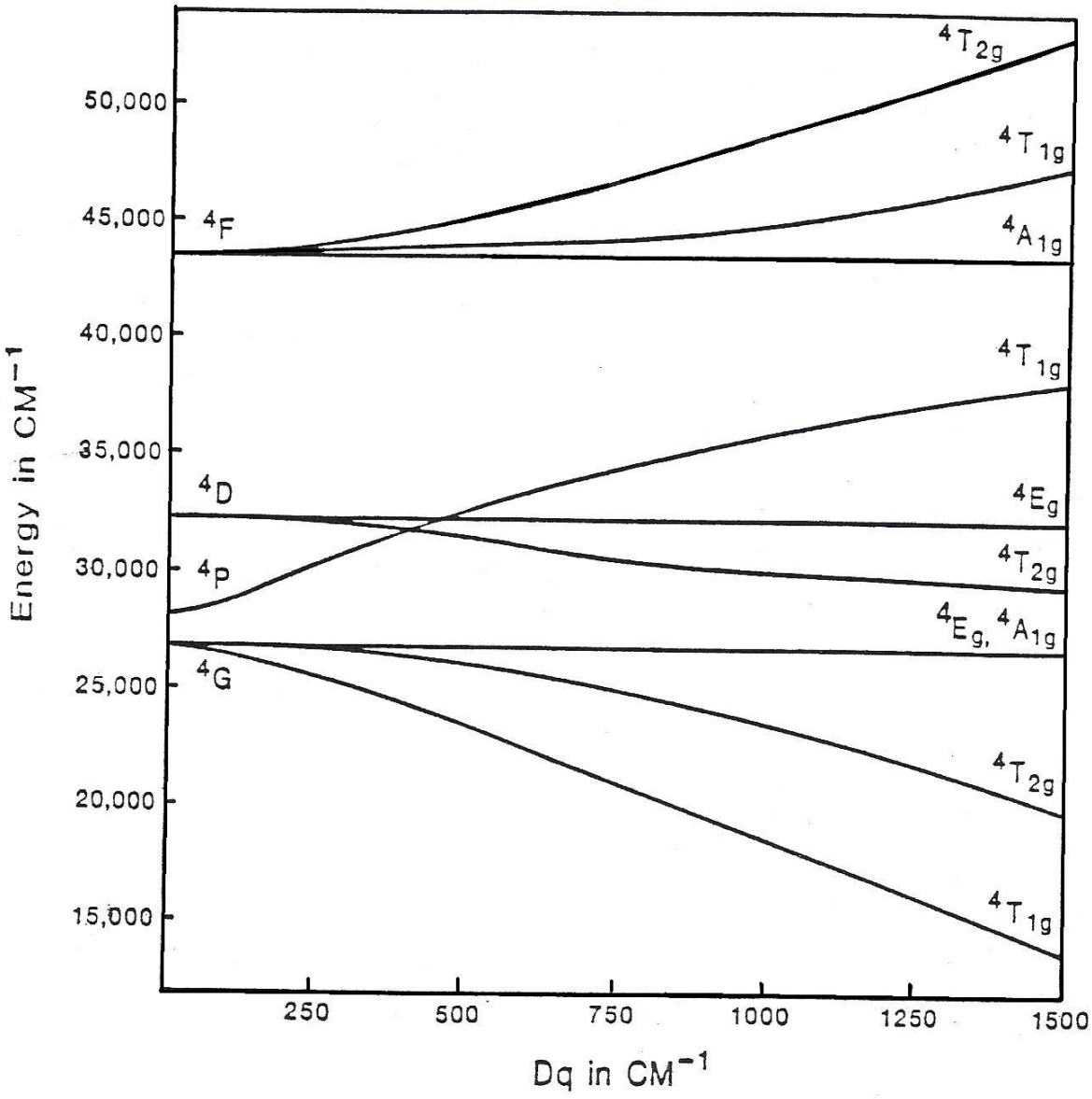

Figure 2.6: The Orgel diagram for Mn^{+2} presents the behavior of the states resulting from the crystal field effect with increasing D_q after Orgel (1953)

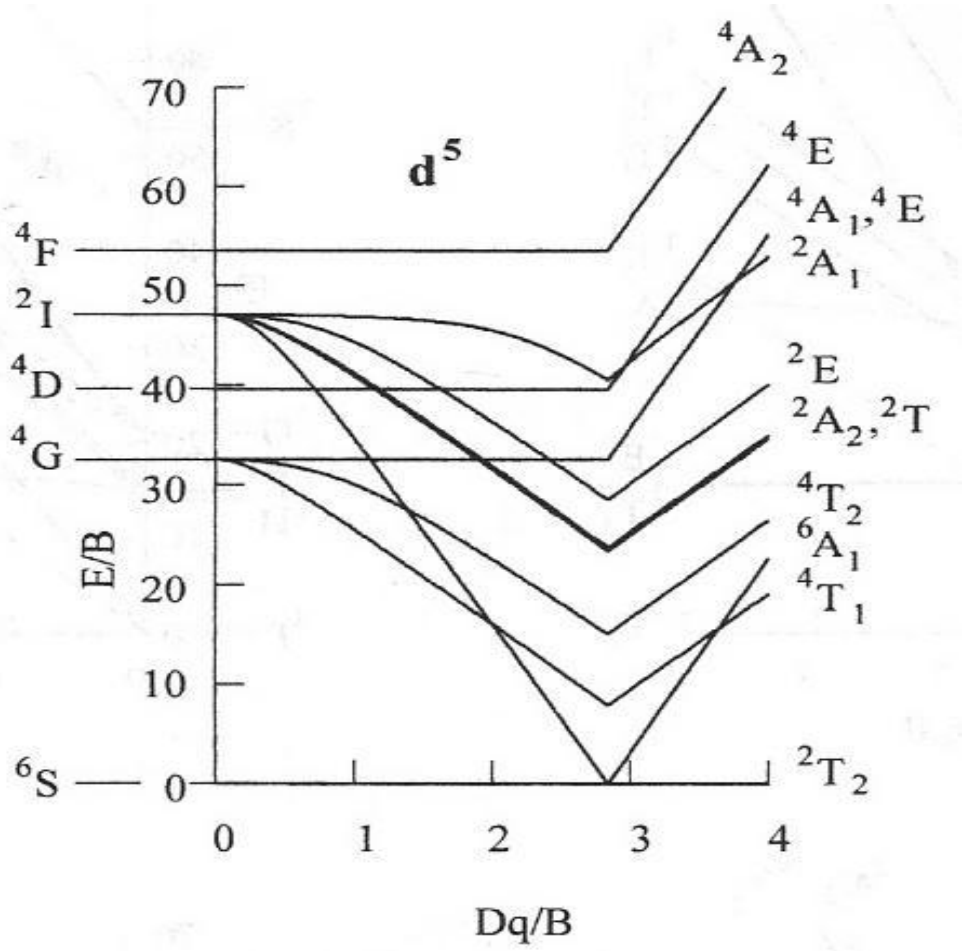

Figure 2.7: The Tanabe-Sugano energy level diagram for d^5 configuration in octahedral coordination after Henderson and Bartram (2000).

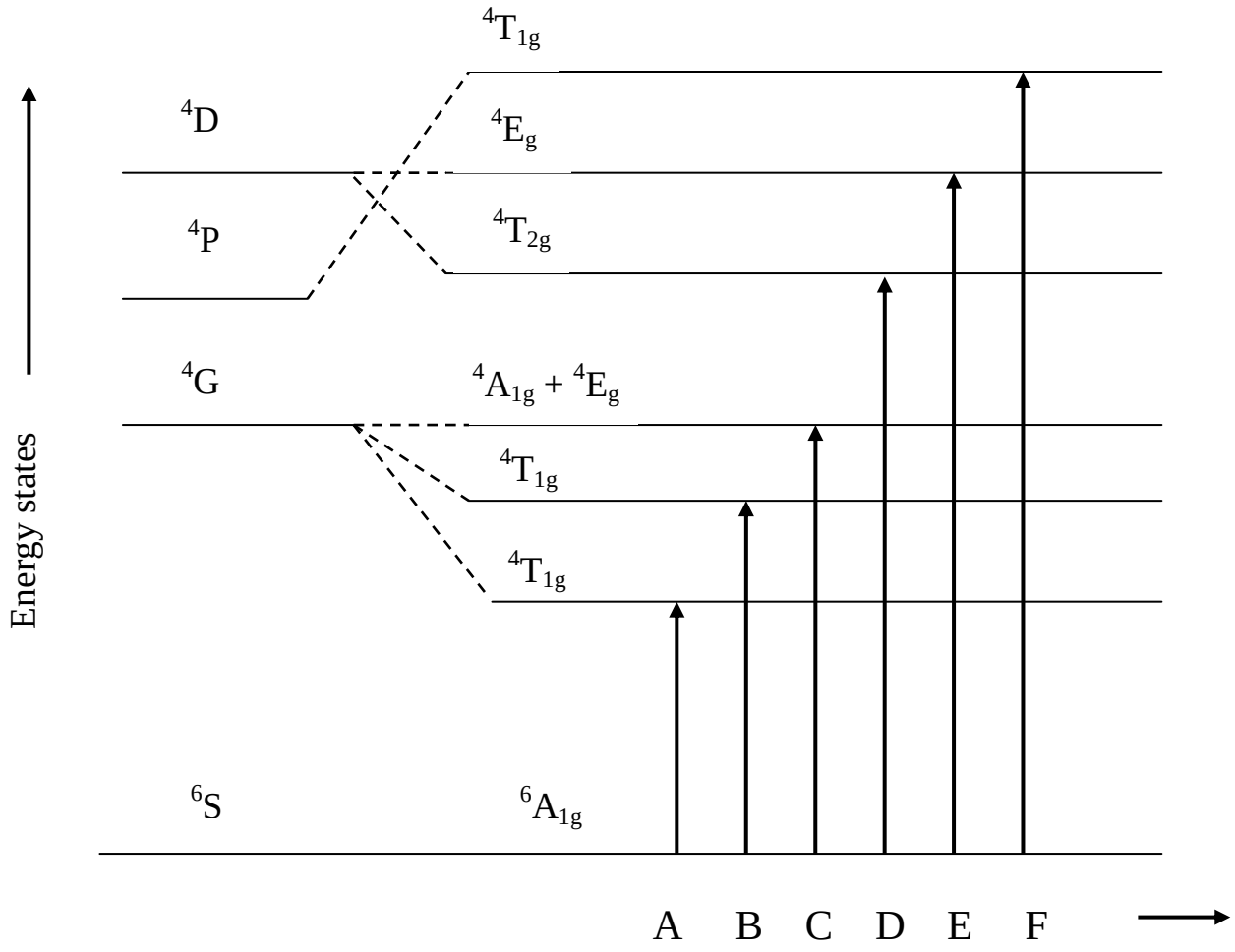

Figure 2.8: The main transition for d^5-levels

2.6 Absorption of Radiation

The change of an electron state in a system comes as a result of absorbing or emitting an amount of energy equal to the energy difference between the two states of the electron. The change of energy is a direct result of the interaction with the electromagnetic radiation, which includes electric and magnetic field.
When electromagnetic radiation falls on the central ion of the magnetic crystal, the electric field interacts with the electric dipole of the ion. This interaction is treated as a time dependence perturbation term added to the original Hamiltonian of the system (Slater, 1960).

$$H = H_o + H_{\text{int}}(t) \qquad 2.14$$

where H_o is divided into two terms. The first term, H_{atom}, consists of the kinetic energy of the electrons and the coulomb potential energy of the electrons in the nucleus field, while the second term, H_{field}, gives the energy of the radiation field. $H_{\text{int}}(t)$ is the important term for our discussion in this section because it describes the interaction between the charged particles and the electromagnetic field, and gives the emission or absorption of photons (Majumdar, 1995):

$$H_{\text{int}}(t) = \sum_i^N \left(-\frac{e_i}{m_i c}\vec{A}(r_i,t).\vec{P}_i + \frac{{e_i}^2}{2m_i c^2} A^2(r_i,t)\right) \qquad 2.15$$

where m_i is the mass of the i^{th} particle, e_i its charge, $\vec{P}_i$ its momentum, and $\vec{A}(r_i,t)$ is a magnetic vector potential at position r_i.

The magnetic vector potential is very small, so the A^2 term is negligible compared with that in A, and may be ignored. Thus we need to consider only the interaction linear term in A (Slater, 1960).

The $\vec{A}.\vec{P}$ term gives emission or absorption of a single photon, the probability of a transition involving a single photon is proportional to the fine structure constant ($e^2/\hbar c \approx 1/137$) (Majumdar, 1995).
The vector potential $\vec{A}$ can be expressed as:

$$\vec{A}(\vec{r}_i,t) = \vec{A}_o\, e^{i\left(\vec{k}.\vec{r}_i - \omega t\right)} \qquad 2.16$$

If the wavelength of the incident radiation or emitted radiation is large compared with the dimensions of the atom (k.r, which is of order 10^{-3} in the case of visible light) (Henderson and Bartram, 2000), so that k.r<<1 and the exponential $e^{ik.r}$ expanded in Taylor series as follows:

$$\vec{A}(r_i,t) = \vec{A}_o\, e^{-i\omega t}\left[1 + i\vec{k}.\vec{r}_i + \frac{\left(i\vec{k}.\vec{r}_i\right)^2}{2} + \ldots\right] \qquad 2.17$$

The first term in the expansion is:

$$\frac{e_i}{m_i c}(\vec{A}_o.\vec{P}_i)e^{-i\omega t} \qquad 2.18$$

If the transition occurs between two states a and b, the contribution of the first term to the perturbation H_{int} (t) in terms of H_{int}' (t) as follows:

$$H'_{\text{int}}(t) = \left(\frac{e_i}{m_i c}\vec{A}_o \cdot \langle b|\vec{P}_i|a\rangle\right)e^{-i\omega t} \qquad 2.19$$

where, $P_i = \frac{im_i}{\hbar}[H, r_i]$, then

$$H'_{\text{int}}(t) = \frac{ie_i A_o}{c\hbar}\cdot\left[\langle b|H r_i - r_i H|a\rangle\right] = \frac{ie_i A_o}{c\hbar}\cdot\left[\langle bH|r_i|a - \langle b|r_i|Ha\rangle\right] \qquad 2.20$$

$$H'_{\text{int}} = \frac{iA_o}{c}\frac{(E_b - E_a)}{\hbar}\cdot\left[\langle b|e_i r_i|a\rangle\right] \qquad 2.21$$

$$H'_{\text{int}}(t) = \left(\frac{i\omega_{ba}}{c}A_o.\langle D\rangle_{ba}\right)e^{-i\omega t} \qquad \text{, where } \omega_{ba} = \frac{E_b - E_a}{\hbar}$$

$$H'_{\text{int}}(t) = \left(\frac{E_o}{c}\cdot\langle D\rangle_{ba}\right)e^{-i\omega t} \qquad 2.22$$

where $E_0 = i\omega_{ba}A_0$ and $D(= e_i\vec{r}_i)$ is the electric dipole moment. The above expression is labeled as the electric dipole transition. Since r is an odd function, the matrix elements for the electric dipole moment $\langle D\rangle_{ba}$ have non-zero values only if a and b are two states of opposite parity.

The second term $i\vec{k}.\vec{r}$ of the Taylor series gives two terms, the magnetic dipole moment and electric quadrupole moment whose rates are several orders smaller than the electric dipole rate. The second term of the vector potential can be written as:

$$\vec{A}(r_i,t) = (i\vec{k}.\vec{r}_i)A_o\, e^{-i\omega t} \qquad 2.23$$

This term contributes to the perturbation H_{int} (t) as follows (Blatt and Weisskopf, 1952, Powell and Crasemann, 1961):

$$H''_{\text{int}}(t) = \frac{ie_i}{m_i c}\left(\vec{k}\cdot\vec{r}_i\right)\left(\vec{A}_o\cdot\vec{P}_i\right)e^{-i\omega t} \qquad 2.24$$

$$\left(\vec{k}\,.\,\vec{r}_i\right)\left(\vec{A}_0\,.\,\vec{P}_i\right) = \frac{1}{2}\left[\left(\vec{k}\,.\,\vec{r}_i\right)\left(\vec{A}_0\,.\,\vec{P}_i\right) - \left(\vec{k}\,.\,\vec{P}_i\right)\left(\vec{A}_0\,.\,\vec{r}_i\right)\right] + \frac{1}{2}\left[\left(\vec{k}\,.\,\vec{r}_i\right)\left(\vec{A}_0\,.\,\vec{P}_i\right) + \left(\vec{k}\,.\,\vec{P}_i\right)\left(\vec{A}_0\,.\,\vec{r}_i\right)\right]$$

$$= \frac{1}{2}\left[\left(\vec{k}\times\vec{A}_0\right).\left(\vec{r}_i\times\vec{P}_i\right)\right] - \frac{im_i}{2\hbar}K.\left[r_i r_i\,,H\right].A_0 \qquad 2.25$$

The matrix element of the commutators in the last term is given by:

$$\langle b\left|r_i r_i\,,H\right|a\rangle = -\hbar\,\omega_{ba}\,\langle b\left|r_i r_i\right|a\rangle \qquad 2.26$$

If $B_o = i\vec{k}\times\vec{A}_o$, where B_o is the magnetic flux density of electromagnetic radiation then equ. 2.24 can be expressed in the form:

$$H''_{\text{int}}(t) = \left[-\frac{e_i\vec{B}_o}{2m_i c}\cdot\vec{L} - \frac{ie_i}{2c}E_o.K.\langle b\left|r_i r_i\right|a\rangle\right]e^{-i\omega t} \qquad 2.27$$

where the first term is due to the magnetic dipole transition and the second term is the electric quadrupole transition.

There could be three possible transitions as a result of absorption or emission of electromagnetic radiation:

1) Electric dipole transition.
2) Magnetic dipole transition.
3) Electric quadrupole transition.

2.7 Selection Rules

Transition between any two states for an electric dipole operator occurs only if the following matrix element does not vanish.

$$\langle b \left| e\vec{r} \right| a \rangle = e\left[\langle b|x|a\rangle \hat{i} + \langle b|y|a\rangle \hat{j} + \langle b|z|a\rangle \hat{k} \right] \qquad 2.28$$

Here a and b are the wave functions of the initial and final states respectively, and $e\vec{r}$ is an electric dipole moment operator.
For the spherical harmonics (Majumdar, 1995):

$$\begin{aligned} \langle b|x|a\rangle &= \langle b|\, r\sin\theta\cos\Phi|a\rangle = \langle n'|r|n\rangle\langle l'|\sin\theta|l\rangle\langle m_l'|\cos\Phi|m_l\rangle \\ \langle b|y|a\rangle &= \langle b|r\sin\theta\sin\Phi|a\rangle = \langle n'|r|n\rangle\langle l'|\sin\theta|l\rangle\langle m_l'|\sin\Phi|m_l\rangle \\ \langle b|z|a\rangle &= \langle b|r\cos\theta|a\rangle = \langle n'|r|n\rangle\langle l'|\cos\theta|l\rangle\langle m_l'|m_l\rangle \end{aligned} \qquad 2.29$$

From 2.28 and 2.29 we conclude that the dipole moment operator operates only on the position coordinates x, y, or z, and cannot affect the spin state of the ion. It is a general rule for electric dipole transition that it has no effect on spin states. This means for any possible transition, the initial and final states must have the same spin quantum number. Therefore, we have the general selection rules for the electric dipole transition:

$$\begin{aligned} &\Delta l = \pm 1 \\ &\Delta m_l = 0, \pm 1 \\ &\Delta s = 0 \end{aligned} \qquad 2.30$$

Since the electric dipole operator $e\vec{r}$ is an odd operator, transitions occur only between two states of opposite parity. For the d-d transitions they are forbidden because all d-orbitals are partially even function (g) then the transition between any two states arising from d^n-configuration is not allowed. This is in agreement with Laporte rule, which states that the only allowed electric dipole transitions are those between an even state and an odd state (Cotton, 1963). The parity selection rules are relaxed by asymmetry (odd) vibrations of an octahedral complex, which can destroy the spherical symmetry of the central ion and allow the transition.

The second selection rule, states that any transition for which $\Delta S \neq 0$ is spin forbidden for the electric dipole transition. In the case of manganese ion, it has a ground state ($^6A_{1g}$) which is a sextet state. This means for d^5-configuration, all d-d transition are spin-forbidden too. The spin selection rule is overcome by the exchange interaction of the two neighboring ions in the magnetic crystal, or by the spin-orbit coupling, which mixes states of different spin multiplicity.

In both of the magnetic dipole and electric quadrupole transitions, the initial and final states of an atom have the same parity, and each of them is allowed between d^5 levels, although these transitions have very low intensities with respect to electric dipole transition.
The magnetic dipole moment is given by:

$$M = \sum_i \frac{e\hbar}{2m}(l_i + 2s_i) \qquad \text{Even parity.} \qquad 2.31$$

The selection rules for the magnetic dipole transition are (Majumdar 1995):

$$\Delta j = 0, \pm 1 \qquad \text{(Excluding } 0 \rightarrow 0\text{).}$$

$$\Delta l = 0, \pm 1 \qquad \text{(Excluding } 0 \rightarrow 0\text{).} \qquad 2.32$$

The strength of transition is proportional to the square of the matrix element between the initial and final states of the operator of a magnetic dipole moment as follow (Yen and Selzer, 1981). The intensities of these transitions are very small compared to the measured intensities in our case.

$$f_m = \sum_{a,b} \left| \langle b | M | a \rangle \right|^2 \qquad 2.33$$

The electric quadrupole transition, whose strength is relatively small in comparison to the other two kinds of transition, may be written using the electric quadrupole operator as (Jackson, 1998):

$$Q_{ij} = -e \sum_{n:electrons} r_{i,n}\, r_{j,n} - \frac{1}{3} r_n^2\, \delta_{ij} \qquad 2.34$$

The selection rules for this transition are (Henderson and Bartram, 2000):

$$\Delta l = 0, \pm 1, \pm 2 \qquad \text{(Excluding } 0 \rightarrow 0,\ 0 \rightarrow 1,\ 1 \rightarrow 0\text{).}$$

$$\Delta j = 0, \pm 1, \pm 2 \qquad \text{(Excluding } 0 \rightarrow 0,\ 0 \rightarrow 1,\ 1 \rightarrow 0\text{).} \qquad 2.35$$

2.8 Vibronic interaction

It has been noted that electric dipole transitions between the various states arising from d^n-configuration in an octahedral environment are not allowed, because all these states have "gerade" character (even-parity) inherent in the d-orbitals. These transitions become slightly allowed by a mechanism called vibronic coupling that is a coupling of vibrational and electronic wave functions. We assume that vibration of ligands of the octahedral complex that takes place, destroys the center of symmetry, and allows the transitions (Van Vleck, 1939).

The vibronic wave function can be expressed as (Ballhausen, 1962):

$$\Psi_{vibronic} = \Psi_v \, \Psi_e \qquad 2.36$$

where Ψ_v is a vibrational wave function and Ψ_e is an electronic wave function.

From the above expression, any transition occurs between two even electronic states only if one of the two states is mixed with the odd-type vibration and the other state with the even-type vibration.

In the case of octahedral complex depending on octahedral symmetry O_h, there are several normal modes A_{1g}, E_g, T_{2g}, $2T_{1u}$, and T_{2u} as shown in figure 2.9. However, not all of them preserve the element of symmetry (Herzberg, 1945). The normal modes can be divided into two types. Firstly, even-parity distortion A_{1g}, E_g, and T_{2g} retain the inversion center of the perfect octahedron. The second type is odd-parity distortion, T_{1u}, and T_{2u} and destroys the inversion symmetry (Henderson and Bartram, 2000).

To investigate the effect of asymmetrical ligand vibrations, let us suppose that Q represents an asymmetrical vibrational coordinate, and then the crystal field potential can be expanded as (Ballhausen, 1962):

$$V = V_o + Q\left(\partial V/\partial Q\right)_o + \ldots \qquad 2.37$$

where V is the totally symmetric representation, Q and $\partial V/\partial Q$ an odd vibrational mode.
Depending on the first order of perturbation theory, we can mix odd into even functions as follows:

$$\Psi = \psi_g - \frac{Q\int \psi_g \left(\partial V/\partial Q\right)_o \psi_u \, d\tau}{\left(E_u - E_g\right)} \psi_u \qquad 2.38$$

Ψ_g presents the unperturbed “crystal field” wave function, ψ_u an odd parity wave function.

When the two electronic states N and V coupled with the harmonic oscillator (vibrational) wave functions χ_p, and χ_q respectively, then the vibronic (electronic and vibrational) wave functions can be written as:

$$\Psi_{Np} = \Psi \chi_p = \{\psi_g - Q\int[\psi_g (\partial\upsilon/\partial Q)_o \psi_u /(E_u - E_g)]\psi_u d\tau\}\chi_p$$

$$\Psi_{Vq} = \Psi \chi_q = \{\psi_g - Q\int[\psi_g (\partial\upsilon/\partial Q)_o \psi_u /(E_u - E_g)]\psi_u d\tau\}\chi_q \qquad 2.39$$

The probability of electric dipole transition from $_{Np}$ to $_{Vq}$ is given by the formula

$$\left|\boldsymbol{R}_{Np,Vq}\right|^2 = \langle \Psi_{Np} | e\vec{r} | \Psi_{Vq} \rangle^2 \qquad 2.40$$

| er | is an odd operator, and N, V are even electronic wave functions, so the transition is allowed only if the vibrational states p and q differ by one quantum. The total intensity of these electronically forbidden transition increases with temperature. At higher temperature, the stronger bands appear corresponding to large amplitudes of vibration and greater distortions.

The intensity of phonon-assisted transition is proportional to Liehr and Ballhausen (1957) and Malakhovskii and Vasilev (1983).

$$I \propto \coth(h\upsilon/2KT) \qquad 2.41$$

where υ is the frequency of the active odd vibration.

To understand how the forbidden transitions become vibronically allowed we apply the multiplication tables in group theory. As an example let us examine the following electronic transition $A_{1g} \rightarrow T_{1g}$ (forbidden transition) given by the direct product representation of Ψ'_e (x, y, z) Ψe. The coordinates x, y, and z transform as a basic for the T_{1u} representation of O_h, so $A_{1g} \rightarrow T_{1g}$ can be written as follows:

$$\Gamma\,[\psi_e'(x, y, z)\,\psi_e] = T_{1g} \times T_{1u} \times A_{1g} = T_{1g} \times T_{1u} = A_{1u} + E_u + T_{1u} + T_{2u} \qquad 2.42$$

Thus, $A_{1g} \rightarrow T_{1g}$ is not allowed because the result of the previous direct product does not contain A_{1g}. But by the simultaneous excitation of a vibration of T_{1u} or T_{2u} symmetry these transition becomes allowed.

$$T_{1u} \times T_{1u} \times A_{1g} = T_{1u} \times T_{1u} = A_{1g} + E_g + T_{1g} + T_{2g} \qquad 2.43$$

The components of the magnetic dipole and electric quadrupole operators transform as bases for the T_{1g} representation of the magnetic dipole operator L and for the E_g and T_{2g} representation of the electric quadrupole operators $r_i r_j$ of O_h (Cotton, 1963).
The two operator's magnetic dipole and electric quadrupole are even under inversion, and they mediate transitions between states of the same parity (Henderson and Bartram, 2000).

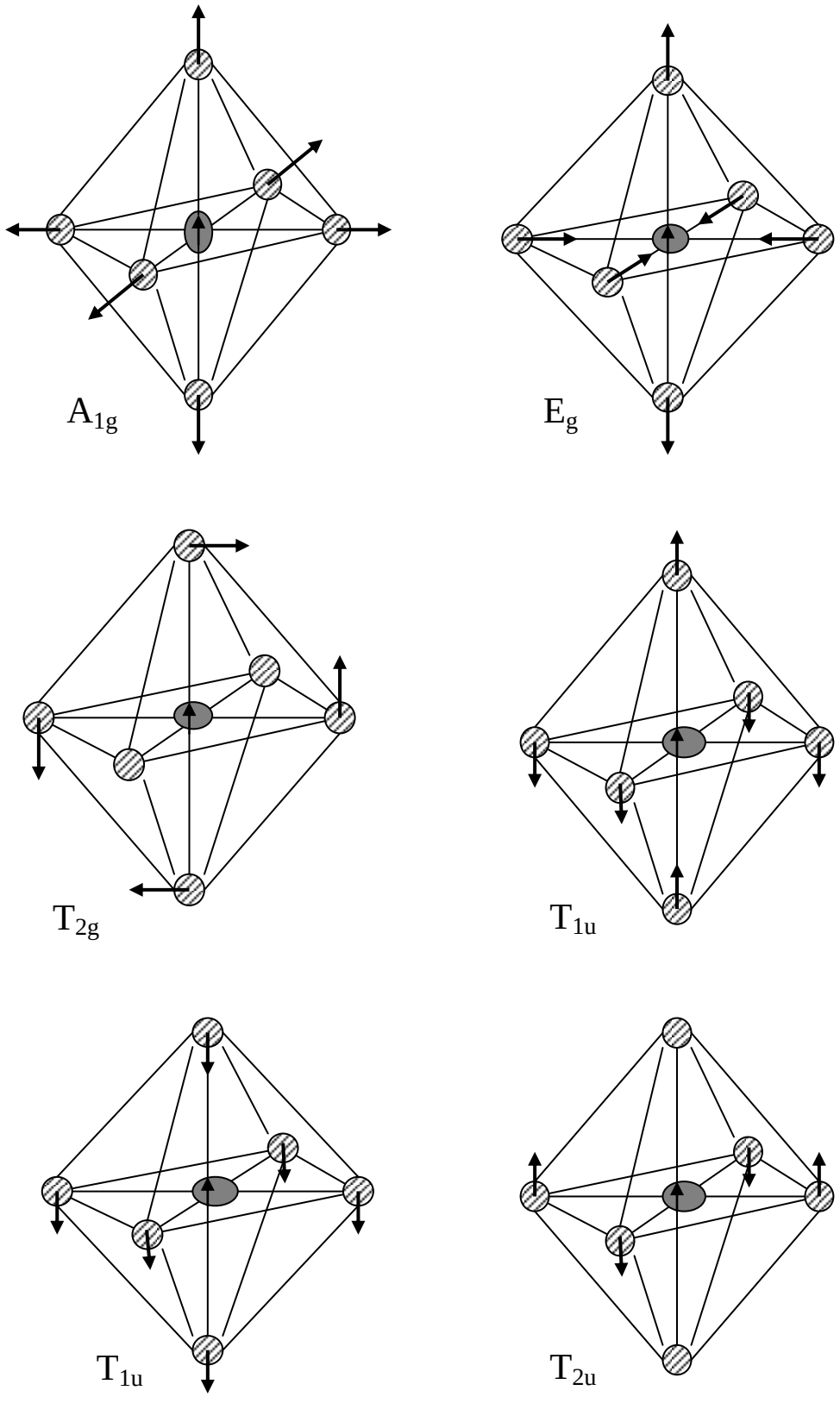

Figure 2.9: The normal modes of distortion of octahedral complex after Henderson and Bartram (2000).

Table 2.3: Multiplication Table for octahedral group after Tinkham, (1964).

	A_{1g}	A_{2g}	E_g	T_{1g}	T_{2g}	A_{1u}	A_{2u}	E_u	T_{1u}	T_{2u}
A_{1g}	A_{1g}									
A_{2g}	A_{2g}	A_{1g}								
E_g	E_g	E_g	$A_{1g}+A_{2g}+E_g$							
T_{1g}	T_{1g}	T_{2g}	$T_{1g}+T_{2g}$	$A_{1g}+E_g+T_{1g}+T_{2g}$						
T_{2g}	T_{2g}	T_{1g}	$T_{1g}+T_{2g}$	$A_{2g}+E_g+T_{1g}+T_{2g}$	$A_{1g}+E_g+T_{1g}+T_{2g}$					
A_{1u}	A_{1u}	A_{2u}	E_u	T_{1u}	T_{2u}	A_{1g}				
A_{2u}	A_{2u}	A_{1u}	E_u	T_{2u}	T_{1u}	A_{2g}	A_{1g}			
E_u	E_u	E_u	A_{1g}	$T_{1u}+T_{2u}$	$T_{1u}+T_{2u}$	E_g	E_g	$A_{1g}+A_{2g}+E_g$		
T_{1u}	T_{1u}	T_{2u}	$T_{1u}+T_{2u}$	$A_{1u}+E_u+T_{1u}+T_{2u}$	$A_{2u}+E_u+T_{1u}+T_{2u}$	T_{1g}	T_{2g}	$T_{1g}+T_{2g}$	$A_{1g}+E_g+T_{1g}+T_{2g}$	
T_{2u}	T_{2u}	T_{1u}	$T_{1u}+T_{2u}$	$A_{2u}+E_u+T_{1u}+T_{2u}$	$A_{1u}+E_u+T_{1u}+T_{2u}$	T_{2g}	T_{1g}	$T_{1g}+T_{2g}$	$A_{2g}+E_g+T_{1g}+T_{2g}$	$A_{1g}+E_g+T_{1g}+T_{2g}$

2.9 Exchange interaction

As a general rule, the optical spectrum of antiferromagnetic ions with an open 3d shell are related to transitions which are forbidden with respect to the spin projection in the single ion approximation. Therefore the transition in the range $^6A_{1g}(^6S) \rightarrow ^4A_{1g}$, $^4E_g(^4G)$ corresponding to C-band is not allowed.
The electric dipole absorption bands are caused by an exchange interaction that involves a transition for a pair of neighboring ions in a magnetic crystal (Popov and Ovchinnikov, 2003). However several research groups have studied in detail the theory of exchange interaction induced electric dipole transitions (Tanabe and Gondaira, 1967, and Ferguson, Guggenheim, and Tanabe, 1966).

To understand how the exchange interaction relaxes the spin selection rule, let the two sublattice models of antiferromagnet MnF_2 initially exist in the ground state with different spin direction where the center ion (denoted as a) has its spin up and the corner ions (denoted as b) have spin down. When absorption of photons takes place, there are three forms of possible interaction between the two ions as shown in the figure 2.10. If the two ions a and b excited to exciton states (exciton is an electronic excited state), the interaction between them is labeled exciton-exciton interaction as presented in figure 2.10b. The second form of interaction is exciton-magnon interaction shown in 2.10c arises when one of the two ions is excited to an exciton state and the other ion is excited to a magnon state (a spin flip) a change in the spin state (Macfarlane and Allen, 1971). On the other hand, figure 2.10d shows the magnon-magnon interaction, produced when the two ions a and b end up in the magnon states.
The operator for exchange induced transition in a pair of ions a and b is (Tanabe and Gondaira, 1967):

$$\mathrm{P}_{ab} = \Pi(ab) S_a . S_b \qquad 2.45$$

where S_a and S_b are spin operators of electrons on ions a and b respectively, and Π is the transition dipole moment.

There are three forms of transition that arise from the exchange coupling as discussed above:

1) Double exciton transition.
2) Exciton-Magnon transition.
3) Double magnon transition.

In these forms of transition the total spin of the two coupling ions must be conserved ($\Delta S = 0$) to break down the spin selection rule and allow the transition.

Consider the case where the final states on opposite sublattices are exciton and magnon states of Mn^{+2}. By using appropriate exciton and magnon wave functions, the transition moment can be written as the following:

$$M = \sum_{n=1}^{N} e^{iK.\delta_{01.n2}} \langle e_{01}\ m_{n2} \left| P^{eff.}_{01,n2} \right| \wp\, g_{01}\ g_{n2} \rangle \qquad 2.46$$

$|e_{o1}\rangle, |g\rangle$ and $|m\rangle$ are single ion wave functions, where g_{01} is the ground state of an ion at the o^{th} site on one sublattice, e_{01} is the excited state at the same site and m_{n2} is spin state of the ground states multiplet (magnon state) for an ion at the n^{th} site on the opposite sublattice. P^{eff} is the effective dipole moment connecting ions $_{01}$ and $_{n2}$, $\delta_{01, n2}$ are the vector from $_{01}$ to $_{n2}$, and $\wp$ is a permutation operator with leads to both direct and exchange terms (Greene, Sell, and White, 1967).

In our case, for the band C, in the o^{th} sublattice the ground state g_{01} has m_s= 5/2 and the excited state e_{01} (m_s= 3/2) on the n^{th} sublattice, the g_{n2} (m_s=-5/2) and m_{n2} (m_s= -3/2). By considering just spin parts, the matrix element given by:

$$\langle \uparrow\uparrow\uparrow\uparrow\downarrow \quad \downarrow\downarrow\downarrow\downarrow\uparrow \left| P_{eff} \right| \uparrow\uparrow\uparrow\uparrow\uparrow \quad \downarrow\downarrow\downarrow\downarrow\downarrow \rangle$$

From the above exchange state between opposite sublattice, we can overcome the spin selection rule and the transition becomes allowed.
Depending on the general rule of spin-spin coupling of two ions, we can write an expression of the energies E_s of the two neighboring manganese ions due to the exchange interaction between them in the absence of applied magnetic field as follows (Hoekstra, Boudewijn, Groenier, and Hass, 1983 and Van Vleck, 1932):

$$E_S = -2K S_a . S_b \qquad 2.47$$

$$E_S = -K\left[S(S+1) - S_a(S_a+1) - S_b(S_b+1)\right] \qquad 2.48$$

.
where S is the total spin of the two ions $S = S_a + S_b$, and K is the exchange coupling constant.

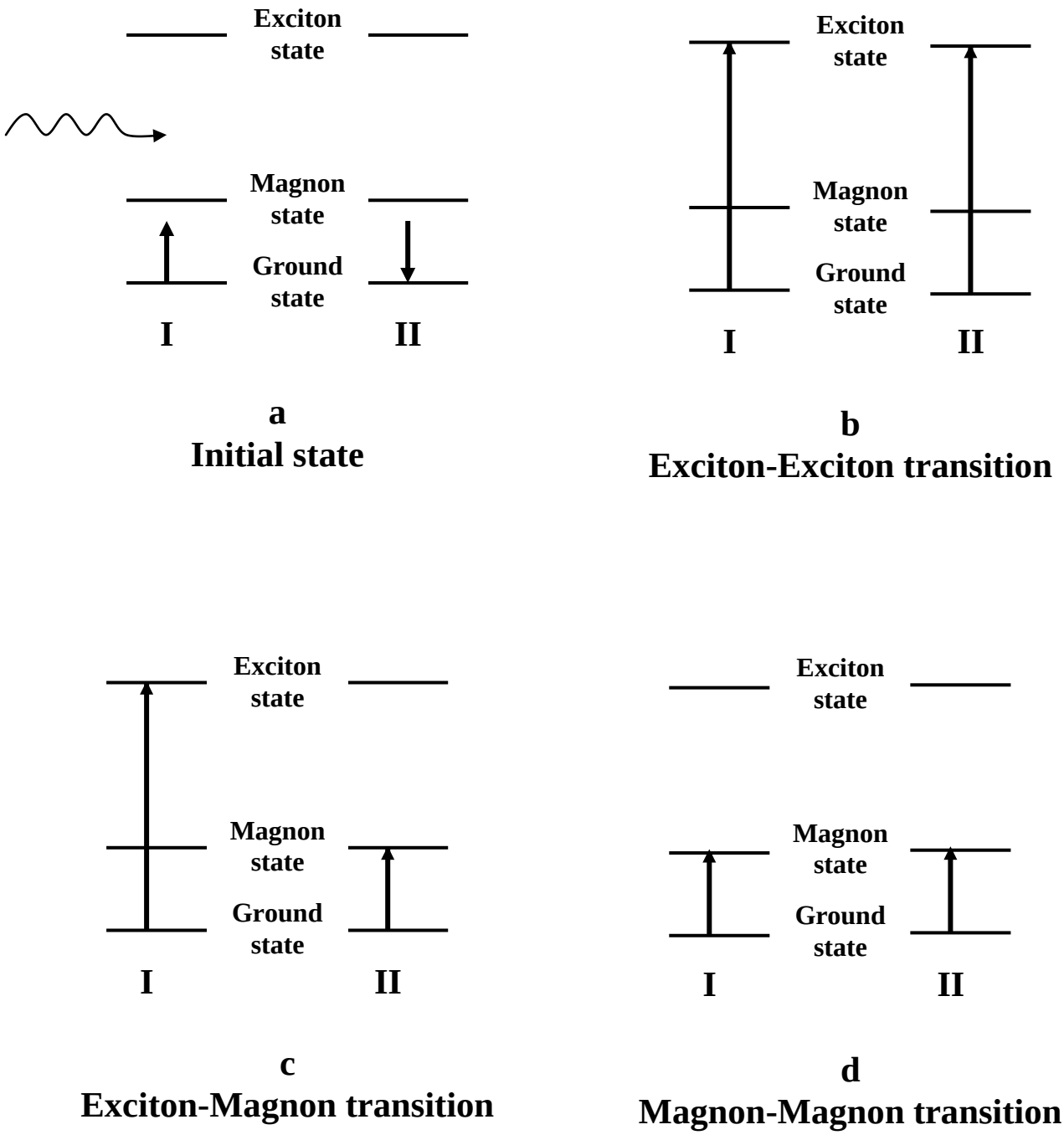

Figure 2.10: Scheme of the exciton-magnon, exciton-exciton, and magnon-magnon transitions between the nearest two sublattices I and II after Eremenko, Karachevtsev, Kazachkov, Shapiro, and Slavin (1993)

Chapter Three

Experimental data

3.1 Introduction

The data used in this work were obtained by Darwish, Abumansoor and their colleagues at West Virginia University labs in the USA.

Measurements were carried out using several samples of MnF_2, $RbMnF_3$, and $KMnF_3$ with different thicknesses to get different optical densities for the various bands. For MnF_2, two samples were used with thicknesses of 0.0300 cm, and 0.1056 cm. Three samples were used for $RbMnF_3$ with thicknesses of 0.1801 cm, 0.0601 cm, and 0.0260 cm. Four samples were used for $KMnF_3$ with thicknesses 0.1199 cm, 0.3025 cm, 0.0500 cm, and 0.025 cm.
Each sample was cleaned with acetone and fixed over a small hole in a plate made of Oxygen-Free-High-Conductivity (OFHC) copper. The copper plate is fastened to the sample holder by a set of screws and surrounded by special low temperature grease.

All the spectroscopic measurements reported here were carried out on the Cary 14 spectrophotometer. The Model 14 spectrophotometer is designed for automatic recording of absorption spectra in the wave length 1860 Å - 26000 Å with a good resolving power and high photometric accuracy.

The light sources of the instrument are a hydrogen lamp for the ultraviolet region, and tungsten lamp for the visible and infrared regions. The energy detectors are a 1p28 multiplier phototube for the ultraviolet and visible regions, and a lead sulfide cell for the infrared.

To obtain the required measurements of this experiment, the sample had to be cooled and kept at constant temperature for a reasonable time to perform the necessary scanning, and to avoid the formation of frost along the path of light. All these requirements were met by the Air Product Model CSA - 202A Displex Closed Cycle Refrigeration system.

3.2 Experimental procedure:

After calibration of the system by developing the spectra of a known standard sample (Holmium Oxide), the data was recorded for the temperature range between10 K and 300 K. When the coldest possible temperature was reached at about 10 K, the stabilization was done with the help of the digital temperature controller and the scan was made. The next data set was taken after the temperature increases slowly until the desired temperature is reached and stabilized. The scanning procedure was repeated several times until reaching room temperature.

3.3 Bands assignments

The observed bands in the 2000 – 6000 Å range were identified with transition from $^6A_{1g}$ (^6S) ground state to various quartet excited states of Mn^{+2}, as listed in table 3.1. The assignments of these bands are A, B, C, D, E, and F…from the longer to shorter wave length in the visible and near ultraviolet regions as shown in figure 3.1. The bands A and B are exciton-magnon-phonon bands, and the remaining bands are exciton-magnon bands. Other bands appear and are labeled as double-exciton bands as α and β bands corresponding respectively to (A+A) band and (A+B) band (Fujiwara and Tanabe, 1972, Shinagawa and Tanabe, 1971, and Tsuboi and Kleemann, 1983). Other double exciton bands as γ (A+C) reported later (Darwish and Seehra, 1988).

Several investigation of these bands were carried out through dealing with temperature dependence of line positions, oscillator strength of the transitions and the effect of applied magnetic field on the bands (Zabluda, Malakhovskii, and Edelman, 1985), (Gurylev, Vereshchagin, Dimitriev, and Kurbatov, 1975) and (Darwish, Seehra, Abumansoor, 1986). This work will concentrate on the fine structure of the C-band

Table 3.1: The line position observed for some of the main bands in MnF_2 at 300 K (Abumansoor, 1985).

Bands	**Transition**	**Observed Energy**
A	$^6A_{1g}(^6S) \rightarrow {}^4T_{1g}(^4G)$	19558 cm^{-1}
B	$^6A_{1g}(^6S) \rightarrow {}^4T_{2g}(^4G)$	23524 cm^{-1}
C	$^6A_{1g}(^6S) \rightarrow {}^4A_{1g}(^4G), {}^4E_g(^4G)$	25183 cm^{-1}
D	$^6A_{1g}(^6S) \rightarrow {}^4T_{2g}(^4D)$	28145 cm^{-1}
E	$^6A_{1g}(^6S) \rightarrow {}^4E_g(^4D)$	30206 cm^{-1}
F	$^6A_{1g}(^6S) \rightarrow {}^4T_{1g}(^4P)$	33069 cm^{-1}

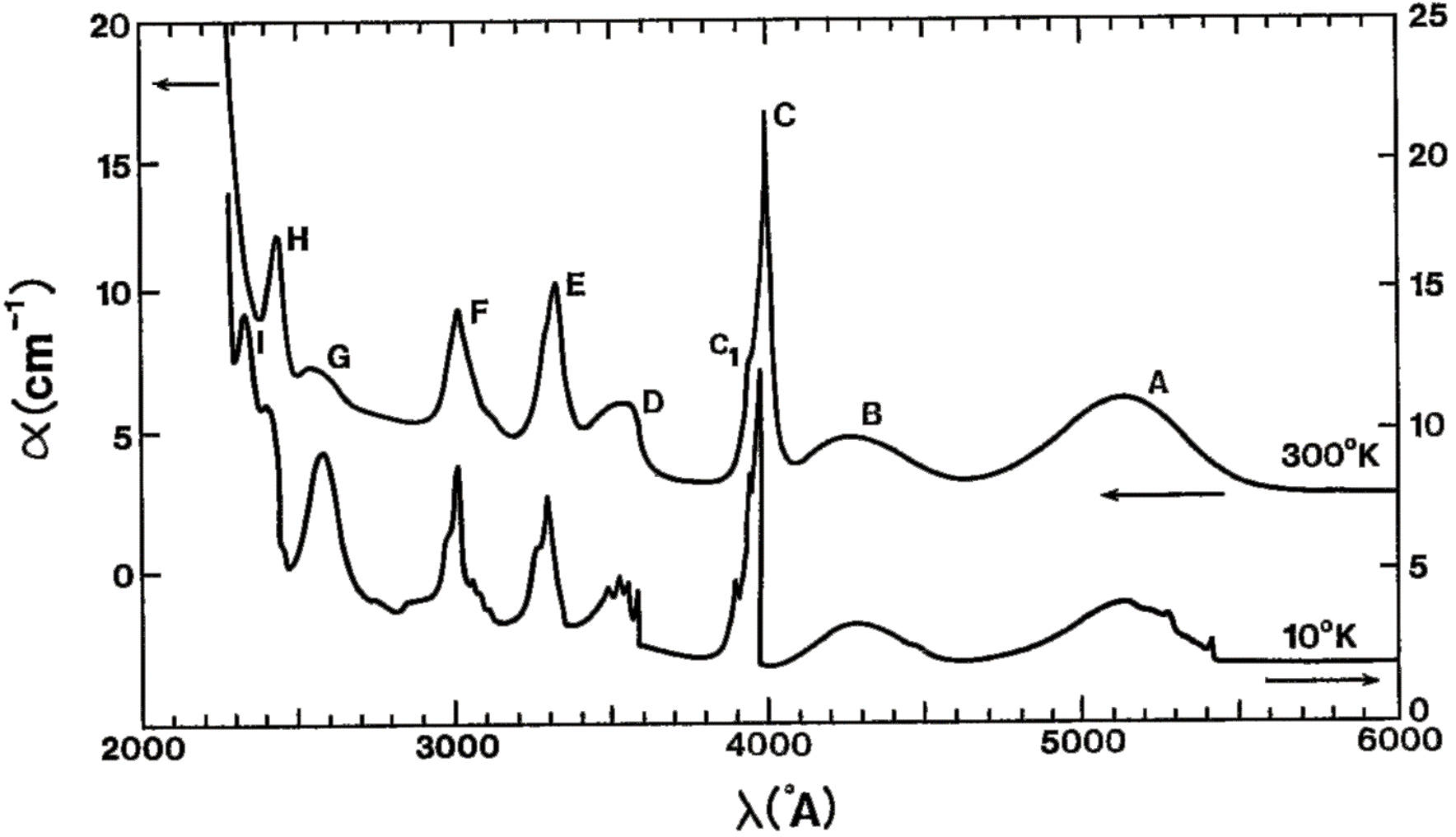

Figure 3.1: Absorption spectrum of MnF_2 crystal at 10 K and 300 K after Darwish, Abumansoor, and Seehra (1986).

3.4 The C-band:

In the case of the C-band ($^6A_{1g}(^6S) \rightarrow {}^4A_{1g}(^4G)$, $^4E_g(^4G)$) it is noted that two kinds of crystal-field transitions are involved in this band to the two levels of $^4A_{1g}$, and ^4E_g, which are degenerate in the crystal field and the spin-orbit coupling does not split them to first order (Wong, Scarpace, Pfeifer, and Yen, 1974).

The line position of the C-band decreases with increasing temperature below T_N, and becomes nearly temperature independent above T_N with negligible phonon effects as shown in figure 3.2. In addition to line position studies, integrated intensity of the band shows a decrease in the intensity below T_N with decreasing temperature and near constant values above T_N as shown in figure 3.3. These features of the band made it easy to label the C-band as pure exciton-magnon band.

The figure 3.2 also shows the temperature dependence of the line position of the F-band, where the two bands C and F have approximately similar behavior below and above T_N. It should be noted that this result is equivalent to that of other exciton-magnon bands, where above T_N the line position and intensity of all of these bands show weak dependence on temperature (Fujiwara, Gebhardt, Petanides, and Tanabe, 1972).

On the contrary, the line positions of A and B bands increases with increasing temperature as shown in figure 3.4. This is consistent with the physical picture in which a phonon is involved and has an effect on the behavior of these bands. These transitions are phonon-assisted transitions and labeled as exciton-magnon-phonon bands. (Darwish, Seehra, and Abumansoor, 1986).

Fig.3.5 shows the data obtained for band C at different temperatures from10 K to 300 K. At 10 K six peaks appear, a few of them are narrow peaks and the remaining peaks are broad. At 60 K near T_N not all of these six bands appear, only four of them are prominent and shifted to lower energy. The best determination of the shifted energy of the C-band is about 57 cm^{-1} from 10 K to 60 K by considering the most dominant peak of the four prominent peaks.

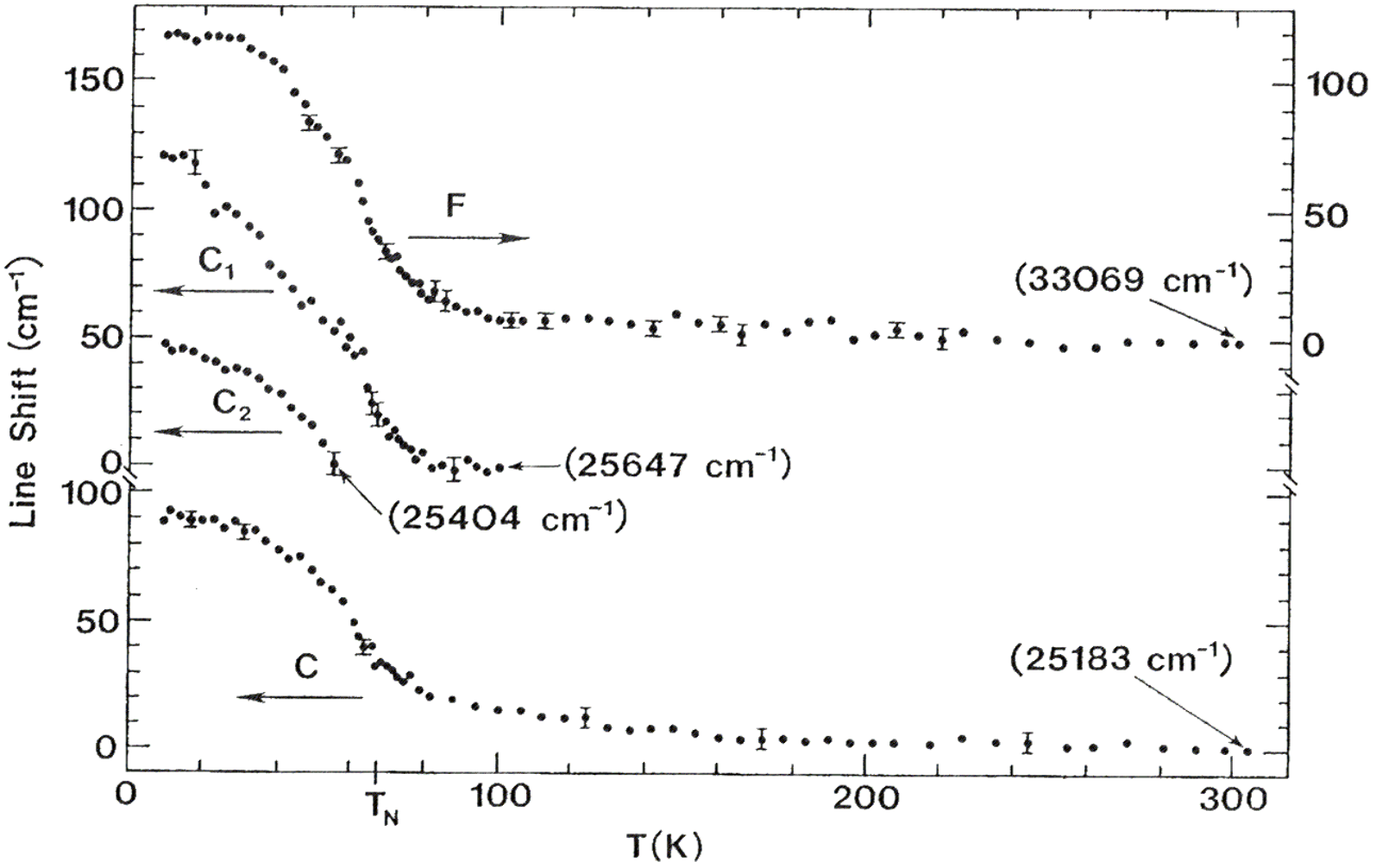

Figure 3.2: Temperature dependence of the line position of C and F bands after Abumansoor (1985).

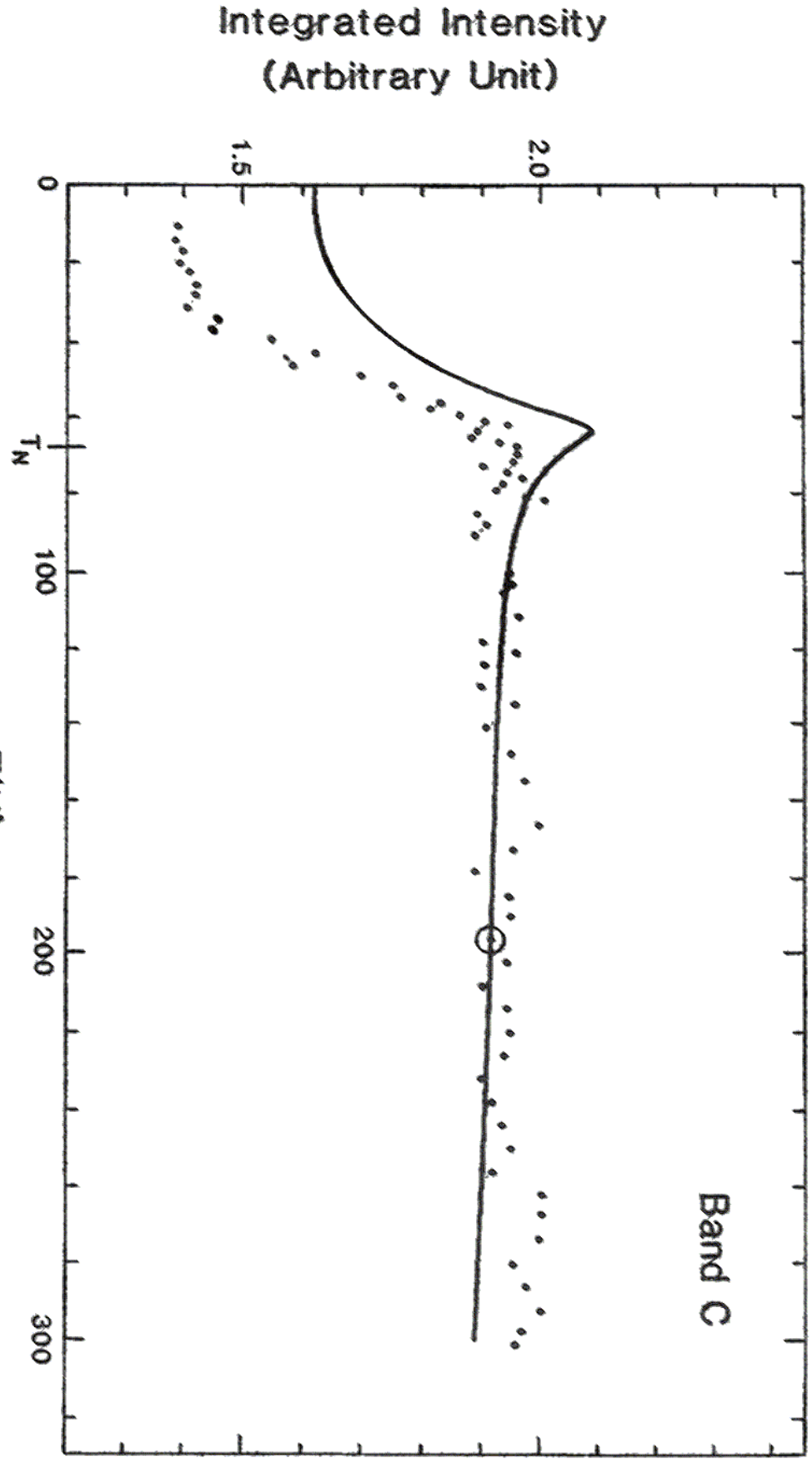

Figure 3.3: Temperature dependence of the integrated intensity of the C-band bellow and above T_N after Abumansoor (1985).

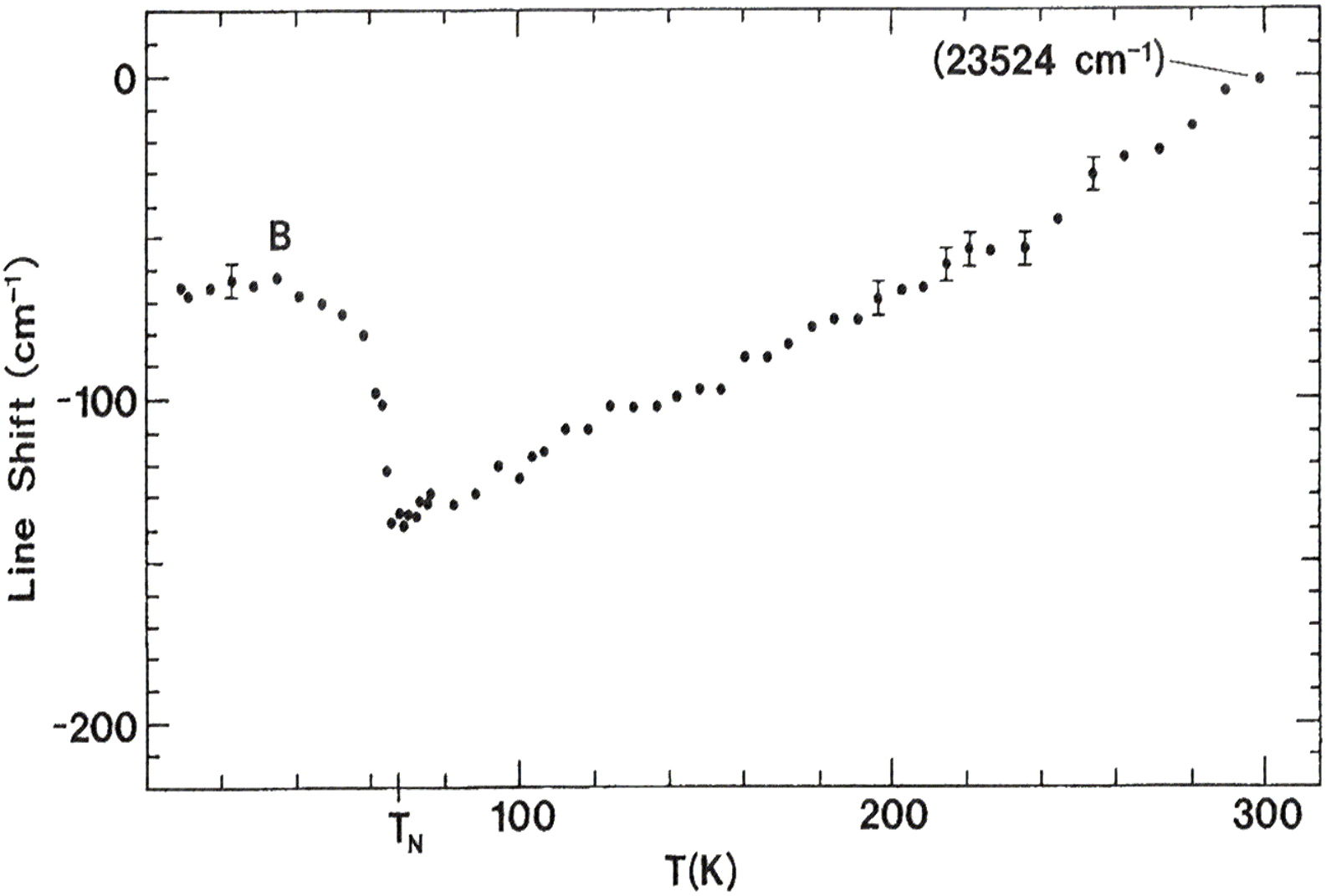

Figure 3.4: Line shift of band B with temperature after Abumansoor (1985).

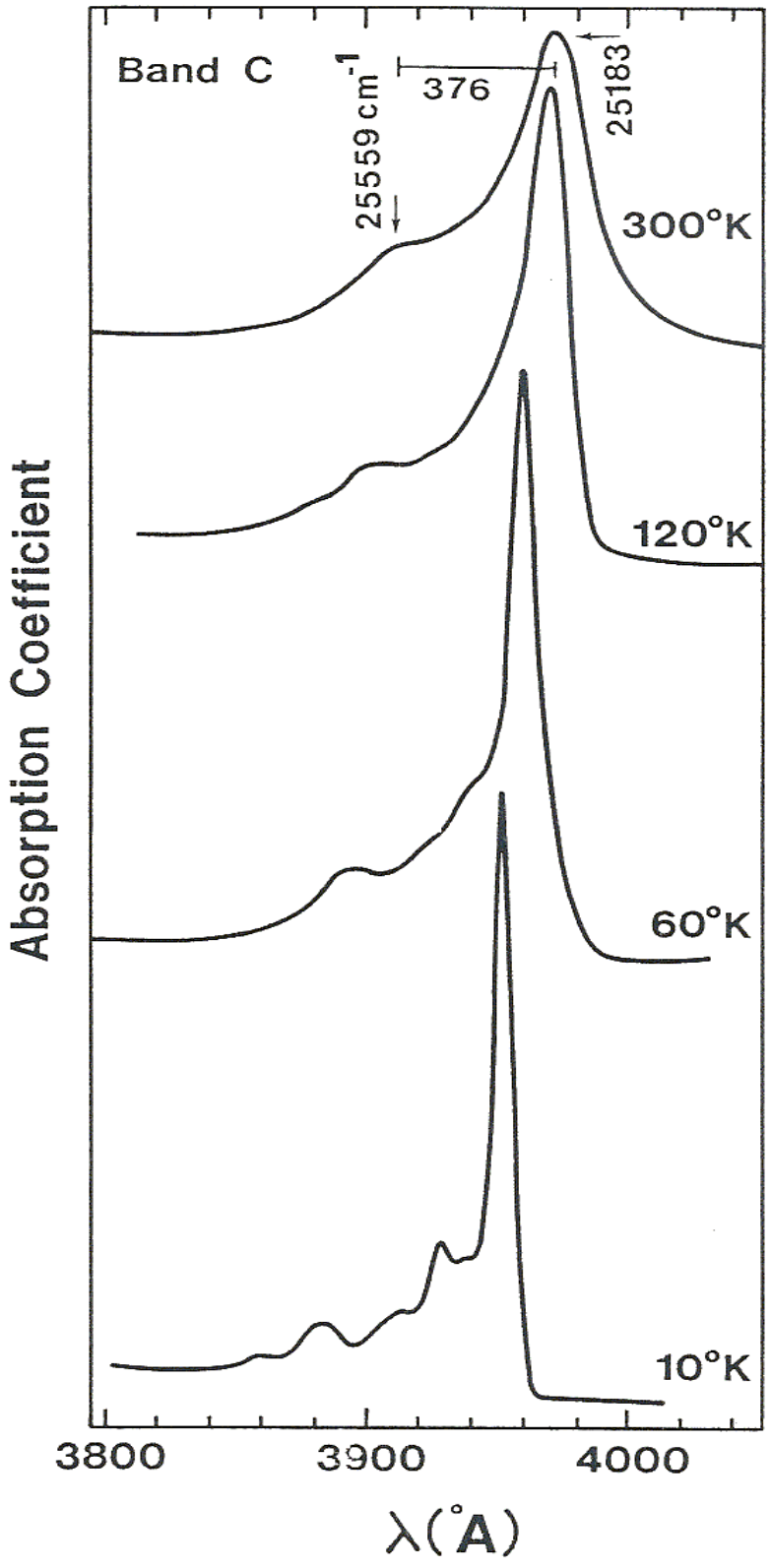

Figure 3.5: Absorption spectrum of the C-band at various temperatures after Abumansoor (1985).

3.5 Fine structure of the C-band

The major goal of this work is to explain the fine structure of the C-band. There are several peaks that appear in the fine structure of the C-band below T_N, as presented in the different experimental data.

The unpolarized spectrum in figure 3.5 of the C-band shows six peaks that appear at 10 K. Some of them are broad implying several lines in each peak. The separation between these lines was easily produced either by decreasing the temperature to less than 10 K or by using polarized spectra as observed in α, σ, and π-spectrum in figure 3.6. In the α-polarized (α-spectrum) the incident light is aligned parallel to the c-axis of the crystal and the electric field is perpendicular to c-axis. In the π-spectrum the incident light is perpendicular to c-axis and the electric field parallel to c-axis. However in the σ-spectrum the incident light and the electric field are perpendicular to c-axis.

From figure 3.6, several peaks appear in the α-spectrum of the C-band at10 K. There is some symmetry noticed in the arrangement of these peaks, which are classified into four groups with each group containing three peaks. Most of these peaks are narrow below T_N, where the spins are ordered and the exchange interaction is a dominant factor at this range of temperature. As the temperature increases all of the peaks become broad and weak. At T_N most of these peaks disappear except for four peaks. Above the Neel temperature the spin goes to a disorder phase and the exchange interaction vanishes as shown in figure 3.5. This result agrees well with the calculations for the case of MnF_2 (Sell, Greene, and White, 1967) which indicates that the energy of the magnon has nearly similar behavior as the sub lattice magnetization with temperature from 0 K to T_N.

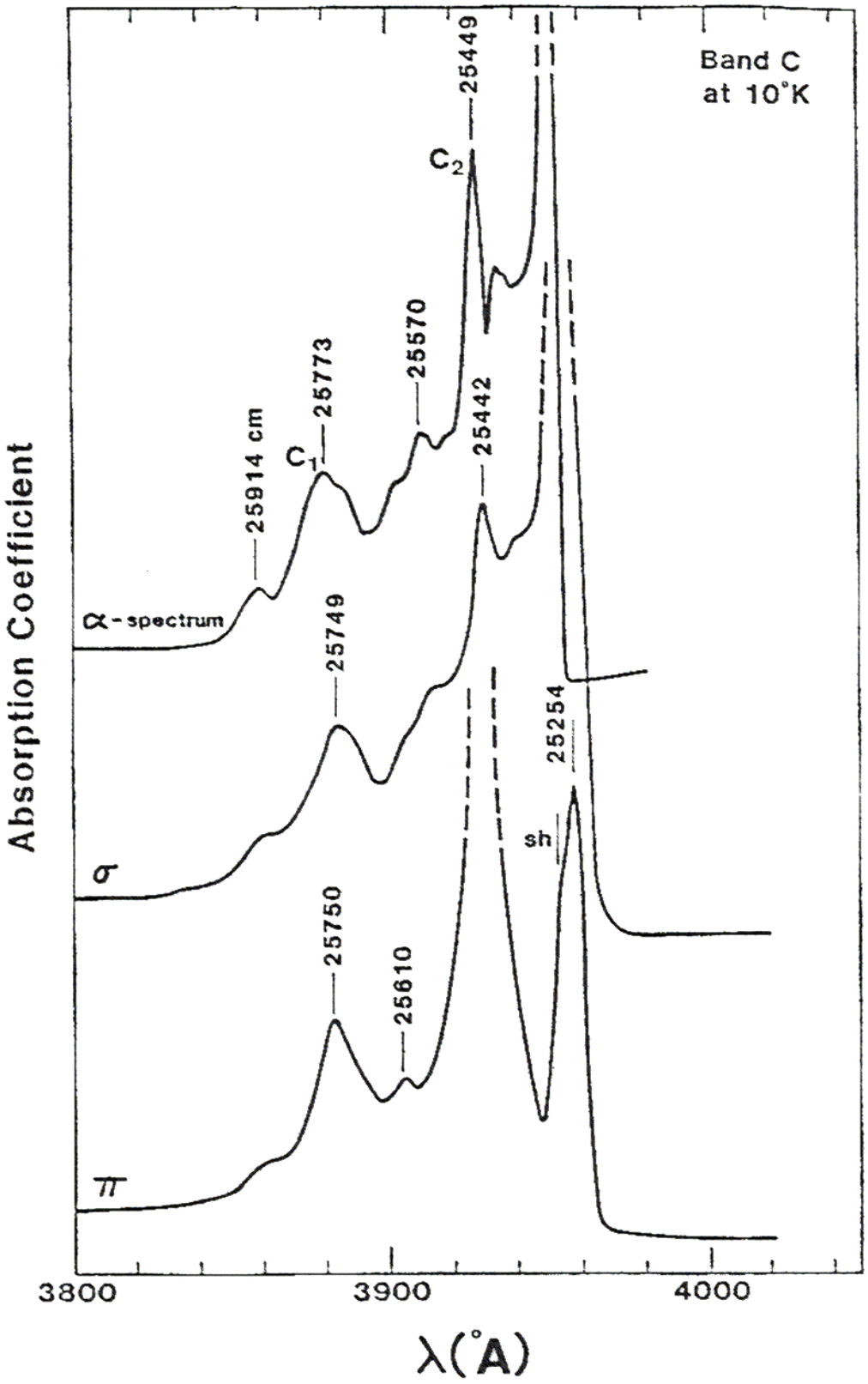

Figure 3.6: The axial (α), σ, and π spectrum of band C at 10 K after Abumansoor (1985).

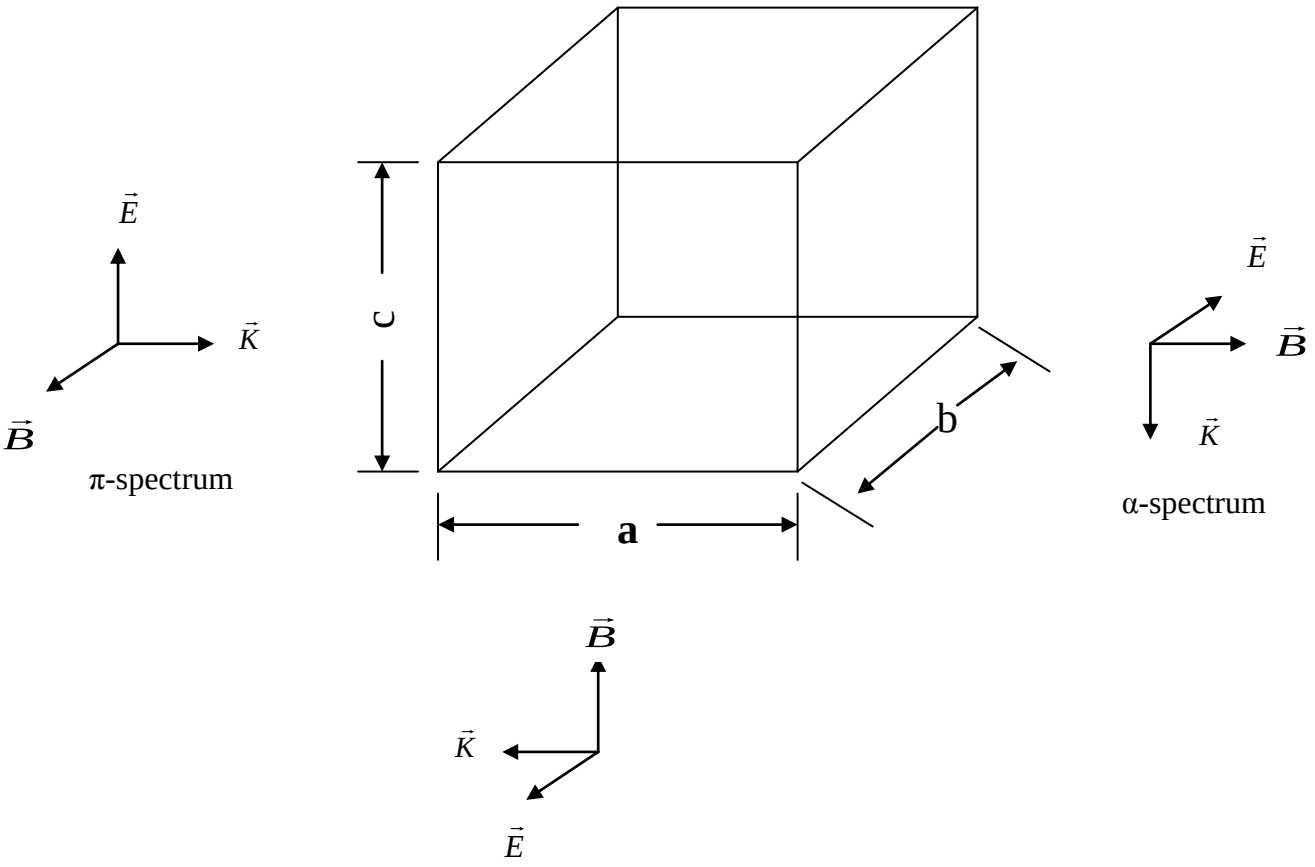

Figure 3.7: The difference between α, σ, and π polarization after Popov (2003) and Popov and Ovchinnikov (2003).

Chapter Four

Theoretical discussion

This chapter is divided into four sections. In the first section a discussion of the allowed and forbidden electric dipole transitions is given. The second section deals with the exchange interaction. The third section discusses the exciton-transitions. The fourth section contains interpretation of spin-spin coupling between the different spin states.

4.1 Allowed and forbidden electric dipole transitions.

There are several energy levels for a free manganese ion ^6S, ^4G, and ^4D…. .These levels split into many states due to the crystal field as shown in figure 2.8. The C-band is the absorption transition between $^6A_{1g}$ (^6S) → $^4A_{1g}$ (^4G), ^4E_g (^4G). Each state splits into several spin states according to its spin multiplicity.

In the paramagnetic phase where there is no effective exchange field, the C-band appears as one sharp peak. Below T_N the spins are ordered and several electric dipole sidebands associated with magnons appear as shown in figure 3.7. To discuss these peaks or sidebands, we need to understand the possible transitions for a single manganese ion. The first possible kind of electronic transitions for a single ion that occur between the states of the same spin-multiplicity, which are called intrasystem combinations. Four possible transitions satisfy the condition for such an intrasystem combinations ($\Delta S = 0$). In the meantime these transitions violate the parity selection rule, since the ground and excited states have even parity and the transitions between the states with the same parity are not allowed. The parity forbiddness is removed by vibronic interaction due to the perturbation of odd vibration into the excited state (Hoekstra and Haas, 1985). The second possible kind of transitions that occur between the states of different spin multiplicity, known as intersystem combinations, and satisfy in the conditions $\Delta S = \pm 1$ that are forbidden for the electric dipole operator due to spin-selection rule (Sugano, Tanabe, and Kamimura, 1970). There are twelve possible transitions satisfy the conditions of the two combinations, their observed energy presented in table 4.1, where C_1, C_2, C_3, and C_4 are the prominent peaks, and the subscript C and H indicate the electric-dipole cold sideband and electric-dipole hot sideband respectively. In a single ion approximation the forbidden transitions may be allowed by spin-orbit and vibronic interactions. The break of the spin and parity selection rules is also possible by the exchange interaction of two manganese ions with opposite sublattices (Hoekstra, Folkersma, and Hass, 1985).

Table 4.1: The observed energy lines of the C-band in MnF_2 compound at 10 K.

Lines type in the C-band	Observed energy lines
C_{1C}	25620 cm^{-1}
C_1	25449 cm^{-1}
C_{1H}	25415 cm^{-1}
C_{2C}	25914 cm^{-1}
C_2	25773 cm^{-1}
C_{2H}	25726 cm^{-1}
C_{3C}	25405 cm^{-1}
C_3	----------
C_{3H}	25315 cm^{-1}
C_{4C}	25570 cm^{-1}
C_4	25561 cm^{-1}
C_{4H}	25515 cm^{-1}

4.2 The role of the exchange interaction

From the previous section, the transitions in cases where $\Delta S = \pm 1$ are forbidden. A possible way to overcome the spin selection rule is to consider the involvement of the two neighboring ions by coupling in an exchange interaction. The exchange mechanism which leaves the total spin unchanged where the spin flip of the exciton (on one sublattice) cancels the spin flip of the magnon (on the other sublattice). Figure 4.1 shows the interaction between the pair of magnetic ions that leads to electric dipole transition. When electronic absorption takes place, the photon virtually excites one ion to an intermediate state of opposite parity (odd state). The exchange interaction between the ions then permits the other ions to be excited to a magnon state while the first ion undergoes a transition to its final state (Sell, 1968). The intermediate state of opposite parity produced by some effects strong enough to destroy the parity selection rule (Malakhovskii, Filimonov, and Goncharov, 1989).

The creation of sidebands can be understood as follows: In spin ordered phase the exchange field develops and lifts the degeneracy of the spin states for the two neighboring manganese ions I and II with up and down sublattices respectively as shown in figure 4.2. The energy gap for the ion where the electronic orbital excitation takes place is denoted by Δe. We assume that the splitting between the different spin states in the ground state is different from that in the excited state. The energy associated with only the spin flips (magnon energy) is denoted by Δe_s. The magnon energy calculated in different works is very small compared to the energy of the transition from one electronic state to a higher electronic excited state (Eremenko, Karachevtsev, Kazachkov, Shapiro, and Slavin, 1993 and Sell, 1968). The sidebands occur in which the first ion has spin component changed by $\Delta S = -1$ and makes a transition to any spin excited state, while a neighboring ion has spin component changed by $\Delta S = +1$ and remains in the ground state, and vice versa. Since the energy differences between the spin states are different from each other, there are twelve possible peak lines with different energies that appear in the fine structure of the C-band as shown in figure 4.2, arranged into four categories. Each category contains three lines ended with similar spin excited state. In each category one of the three lines is a spin-allowed transition; these four lines are labeled as pure exciton lines and will be discussed latter. The other two lines are referred to as the sidebands. These sidebands involve the creation of an exciton and creation or annihilation of a magnon to preserve the spin selection rule. Thus they are sometimes referred to magnon sidebands. The creation of a magnon is named cold sideband, and the annihilation of a magnon is named hot sideband. The cold and the hot sidebands refer to higher and lower energy with respect to the main line.

The number of the peaks from theoretical interpretations approximately agrees well with the experimental data. The experimental data at 10 K showed clearly eleven peaks with the possibility of one of them being resolved into two peaks at a lower temperature.

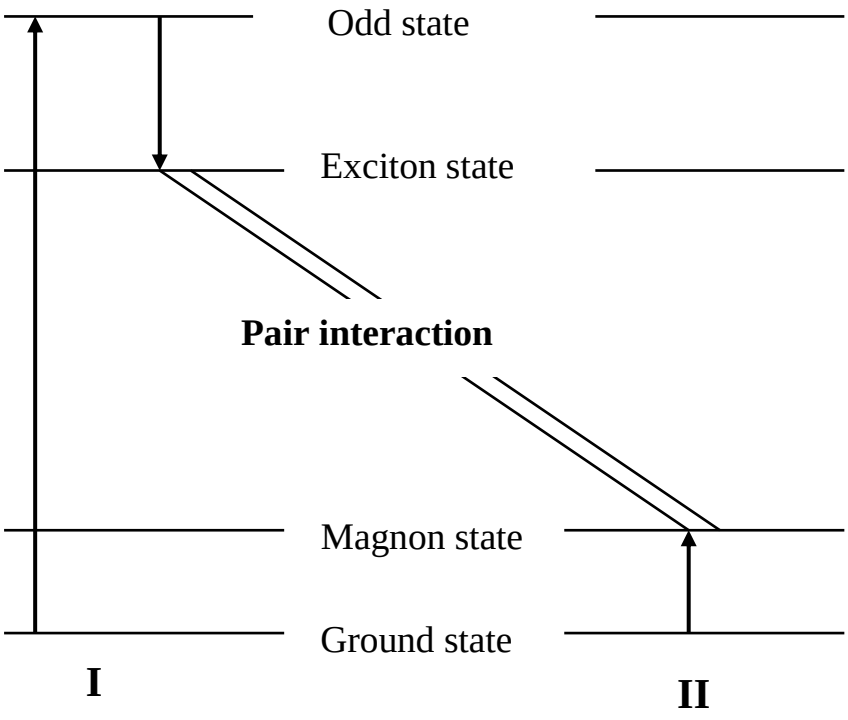

Figure 4.1: Schematic representation of the interaction between a pair of magnetic ions I and II producing magnon sidebands after Sell (1968).

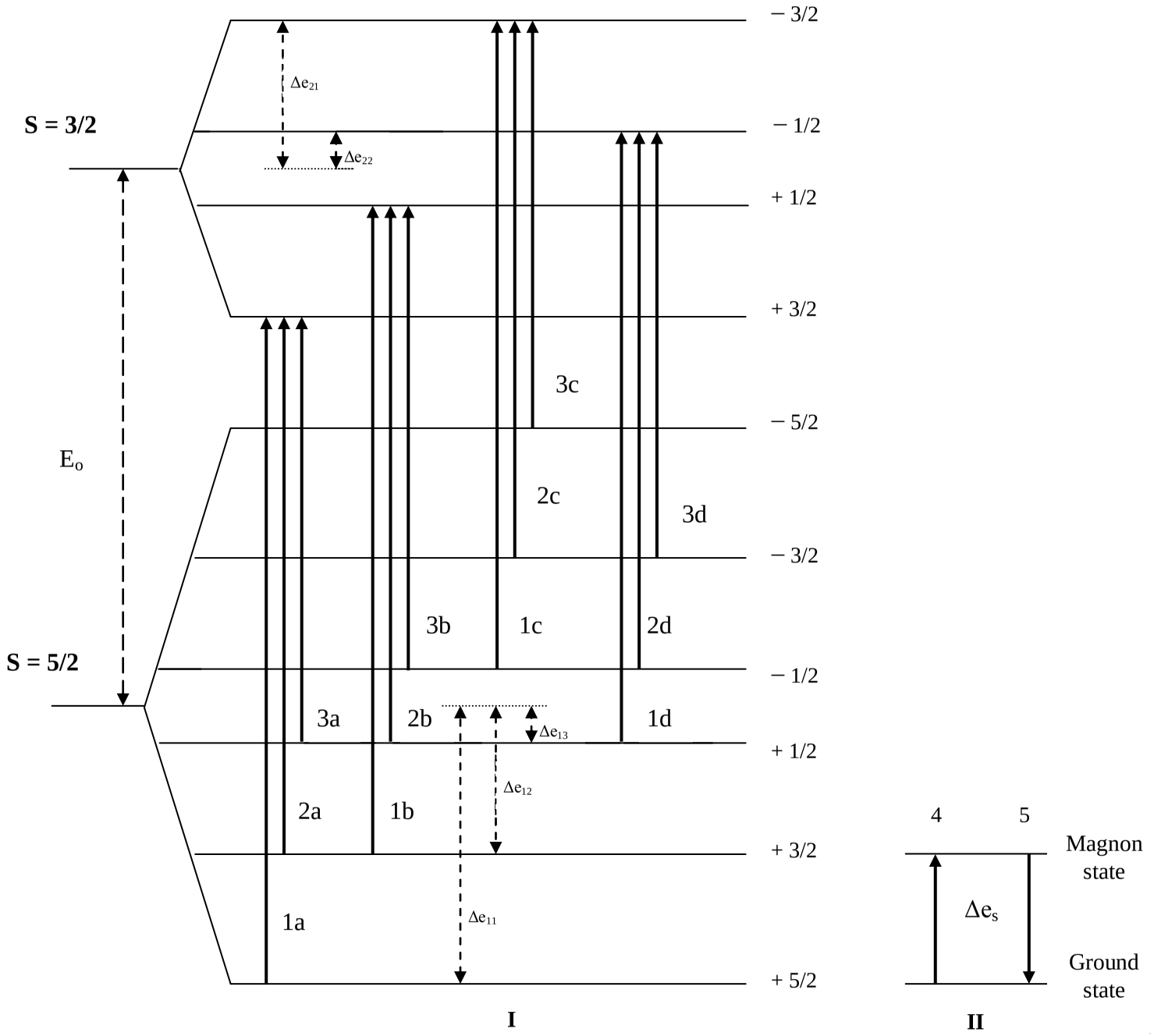

Figur4.2: The four groups of transitions for S = 5/2 in the ground state and S = 3/2 in the excited state with I and II denoting the up and down sublattices, respectively.

The four categories of the twelve transitions are as follows:

1. The first category is a combination of excitations involving two ions that can takes place with wave numbers:

(1a, 4) $E = E_o + \Delta e_{11} - \Delta e_{21} + \Delta e_s$

(2a) $E = E_o + \Delta e_{12} - \Delta e_{21}$

(3a, 5) $E = E_o + \Delta e_{13} - \Delta e_{21} - \Delta e_s$

2. The second category involves the following transitions with wave numbers:

(1b, 4) $E = E_o + \Delta e_{12} - \Delta e_{22} + \Delta e_s$

(2b) $E = E_o + \Delta e_{13} - \Delta e_{22}$

(3b, 5) $E = E_o - \Delta e_{13} - \Delta e_{22} - \Delta e_s$

3. The third group involves these transitions with the corresponding wave numbers:

(1c, 4) $E = E_o - \Delta e_{13} + \Delta e_{21} + \Delta e_s$

(2c) $E = E_o - \Delta e_{12} + \Delta e_{21}$

(3c, 5) $E = E_o - \Delta e_{11} + \Delta e_{21} - \Delta e_s$

4. The fourth group contains these transitions with the corresponding wave numbers:

(1d, 4) $E = E_o + \Delta e_{13} + \Delta e_{22} + \Delta e_s$

(2d) $E = E_o - \Delta e_{13} + \Delta e_{22}$

(3d, 5) $E = E_o - \Delta e_{12} + \Delta e_{22} - \Delta e_s$

4.3 Pure exciton line transitions

There are four transitions that occur between states of the same spin multiplicity. These are labeled as pure electronic transitions for a single ion (also labeled as pure exciton lines). These lines do not violate the spin selection rule and remain prominent at different temperature ranges as shown in figure 3.5. Such lines are noticeable at temperature close to T_N but shift to lower energies according to a change in sublattice magnetization below T_N. The shifted energies for C_1, C_2, C_3, and C_4 (between 10 K and T_N) are 55, 80, 57, and 64 cm^{-1} respectively. The shifted energies at nearly 60 cm^{-1} were obtained by Abumansoor and Seehra (1985) except C_3, where this peak is broad and difficult to determine accurately. The average shifting in their energies corresponds to the shifting of the total C-band.

The four exciton lines correspond to the wave numbers:

$$E = E_o + \Delta e_{12} - \Delta e_{21}$$

$$E = E_o + \Delta e_{13} - \Delta e_{22}$$

$$E = E_o - \Delta e_{12} + \Delta e_{21}$$

$$E = E_o - \Delta e_{13} + \Delta e_{22}$$

The major point to be remembered that these exciton lines violate the parity selection rule, since all the d-states have even parity. Several studies presented different explanation for the relaxation of parity selection rule. The study of Yokogawa, Taniguchi, and Hamaguchi (1977) indicated that the mixing of odd-symmetry phonon state into the even-parity state. Whereas Henderson and Bartram (2000) found that the parity selection rule was overcome by admixture of odd-parity wave functions which associated with higher lying (4p) orbitals into even-parity wave functions. Another explanation presented by Hoekstra, Folkersma, and Haas (1985) indicated that the parity selection rule was overcome by exchange interaction between pairs of manganese ions. Similar exciton-magnon bands may have prominent peaks in their fine structures such as the D and F bands in manganese compounds. Pure exciton lines showed less sensitivity to spin ordering in the antiferromagnetic phase.

4.4 Spin-Spin Coupling

The fine structure of the C-band appears in the antiferromagnet phase below T_N, where most of the peaks become better resolved. Also the number of peak lines for the C-band and the observed energy differences between these lines are approximately the same for different manganese compounds that have the same structure. This supports the proposition that the interaction between the magnetic ions is a dominant factor in the appearance of the fine structure of the C-band. In other words C-band is ideal for the study of the effect of magnetic ordering (Abumansoor and Seehra, 1985).

The electron is a structureless point particle that carries an intrinsic angular momentum S in addition to the extrinsic angular momentum L. Since the spin angular momentum is similar to the orbital angular momentum, all of the L-L, S-S, L-S, and J-J coupling, can be treated in a similar way (Eisberg and Resnick, 1974).

To explain the twelve peaks in the fine structure of the C-band, I follow the same approach proposed by (Eisberg and Resnick, 1974) who did calculate the separation energy between the states arising from spin-orbit interaction by using the Landē interval rule:

$$E = \frac{\lambda}{2}\left[J(J+1) - L(L+1) - S(S+1)\right] \qquad 4.1$$

Here λ is the spin-orbit coupling constant.

In the case of the C-band, all possible transitions occur between states arising from spin multiplicity. So the coupling between these states is spin-spin coupling. By using the expression of exchange energy for the two neighboring ions spin states, we can find the separation energy between different ion spin states as follows (Van Vleck, 1932 and Löwdin, 1962):

$$E_S = 2K\, S_1 . S_2 \qquad 4.2$$

Here K is the exchange coupling factor constant between the spin states, S_1 for the first spin state and S_2 for the second spin state. The total spin states S_1 and S_2 is equal to $S = S_1 + S_2$.

$$S^2 = (S_1 + S_2)^2 = S_1^2 + S_2^2 + 2S_1 . S_2 \qquad 4.3$$

$$S_1 . S_2 = \frac{1}{2}\left[S(S+1) - S_1(S_1+1) - S_2(S_2+1)\right] \qquad 4.4$$

$$E_S = K\left[S(S+1) - S_1(S_1+1) - S_2(S_2+1)\right] \qquad 4.5$$

The magnitude of energy differences between the levels of the sextet ground states is given by:

$$E_S = \left| K\left[S(S+1) - S_1(S_1+1) - S_2(S_2+1)\right] \right| = K\left| \left[20 - \frac{35}{4} - \frac{15}{4} \right] \right| = \frac{15}{2}K$$

where $S_1 = 5/2$, $S_2 = 3/2$, and $S = 4$

While for the case $S_1 = 3/2$, $S_2 = 1/2$, and $S = 2$

$$E_S = K\left| \left[6 - \frac{15}{4} - \frac{3}{4} \right] \right| = \frac{3}{2}K$$

And for the case $S_1 = 1/2$, $S_2 = -1/2$, and $S = 0$

$$E_S = K\left| \left[0 - \frac{3}{4} + \frac{1}{4} \right] \right| = \frac{1}{2}K$$. Figure 4.3 shows the separation energies for the levels due to spin-spin interaction.

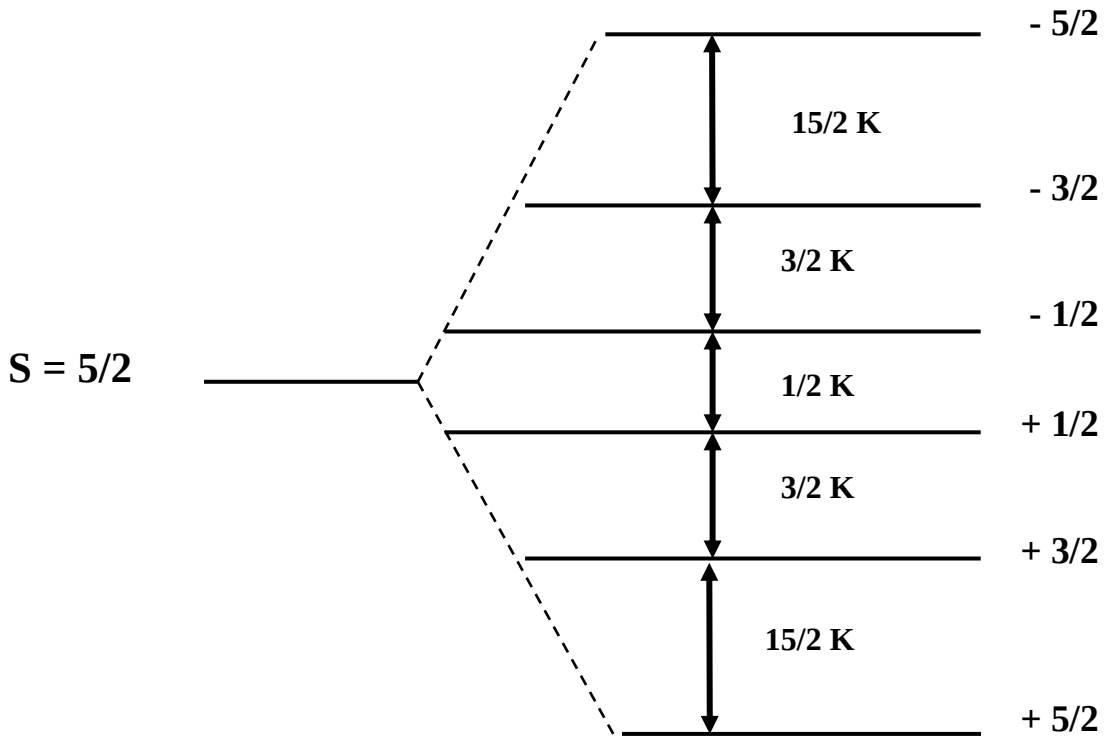

Figure 4.3: The splitting energy of ^{6}S due to spin-spin coupling.

The ratio for every two successive values of energy difference between the spin levels:

$$\frac{E_S(S=5/2\ \&\ 3/2)}{E_S(S=3/2\ \&\ 1/2)}=\frac{15/2}{3/2}=\frac{5}{1}=5:1$$

$$\frac{E_S(S=3/2\ \&\ 1/2)}{E_S(S=1/2\ \&\ -1/2)}=\frac{3/2}{1/2}=\frac{3}{1}=3:1$$

$$\frac{E_S(S=1/2\ \&\ -1/2)}{E_S(S=-1/2\ \&\ -3/2)}=\frac{1/2}{3/2}=\frac{1}{3}=1:3$$

$$\frac{E_S(S=-1/2\ \&\ -3/2)}{E_S(S=-3/2\ \&\ -5/2)}=\frac{3/2}{15/2}=\frac{1}{5}=1:5$$

Table 4.2 shows the experimental data of the ratio for separation energy between the main peaks and the associated two sidebands for three of the four groups.

Table 4.2: The observed energy of the four groups from experimental data.

The groups.	Observed energies of peak lines.	The energies ratios.
The first group	25620 cm^{-1} 25449 cm^{-1} 25415 cm^{-1}	171: 34 ≈ 5 :1
The second group.	25914 cm^{-1} 25773 cm^{-1} 25726 cm^{-1}	141: 47 ≈ 3 :1
The third group.	25405 cm^{-1} --------- 25315 cm^{-1}	--------
The fourth group.	25570 cm^{-1} 25561 cm^{-1} 25515 cm^{-1}	9: 46 ≈ 1 :5

The third group contains only two clear lines which leave the possibility that the most intense line and the most dominant of the spectra may contain two lines, but could not be separated due to limitation of resolution.

We can compare the separation energy calculation by using spin-spin coupling between these lines with the ratios which are listed in table 4.2. The first group in figure 4.2 contains three lines: (1a, 4) and (3a, 5) represent sideband transitions, where (1a, 4) involves creation of an exciton and creation of magnon and (3a, 5) involves creation of an exciton and annihilation of magnon, while (2a) involves creation of exciton. If we neglect the energy associated with magnon transitions in (1a, 4) and (3a, 5) because the magnon energy is very small, then the energy transitions can be written as follows:

(1a): $E = E_o + \Delta e_{11} - \Delta e_{21}$
(2a): $E = E_o + \Delta e_{12} - \Delta e_{21}$
(3a): $E = E_o + \Delta e_{13} - \Delta e_{21}$

These transitions represented by lines from the ground spin states +5/2, +3/2, and +1/2 to the excited spin state + 3/2 respectively as shown in figure 4.4. The calculated values of the ratio between energy gaps for the first group (1a, 2a, 3a) with corresponding to energies (25620 cm^{-1}, 25449 cm^{-1}, 25415 cm^{-1}) is displayed in figure 4.4. Where, line (2a) of energy 25449cm^{-1} is considered the pure exciton line, line (1a) is considered the cold sideband and line (3a) is the hot sideband. In a similar way the ratio between the separation energy between the lines of the second and fourth groups came up to be close to 3 : 1 and 1 : 5 respectively. Strictly speaking, our theoretical explanation agrees well with the experimental data except for the third group which contains two lines with magnitudes of approximately 25405 $cm^{-1}$and 25315 cm^{-1}, the difference between them ≈ 90 cm^{-1}. The third line was not observed, the expectance value of its energy is nearly 25338 to satisfy the third ratio (1: 3) of the spin-spin coupling.
Table 4.3 presents the summary of the experimental data and the theoretical results that have been made for the twelve lines.

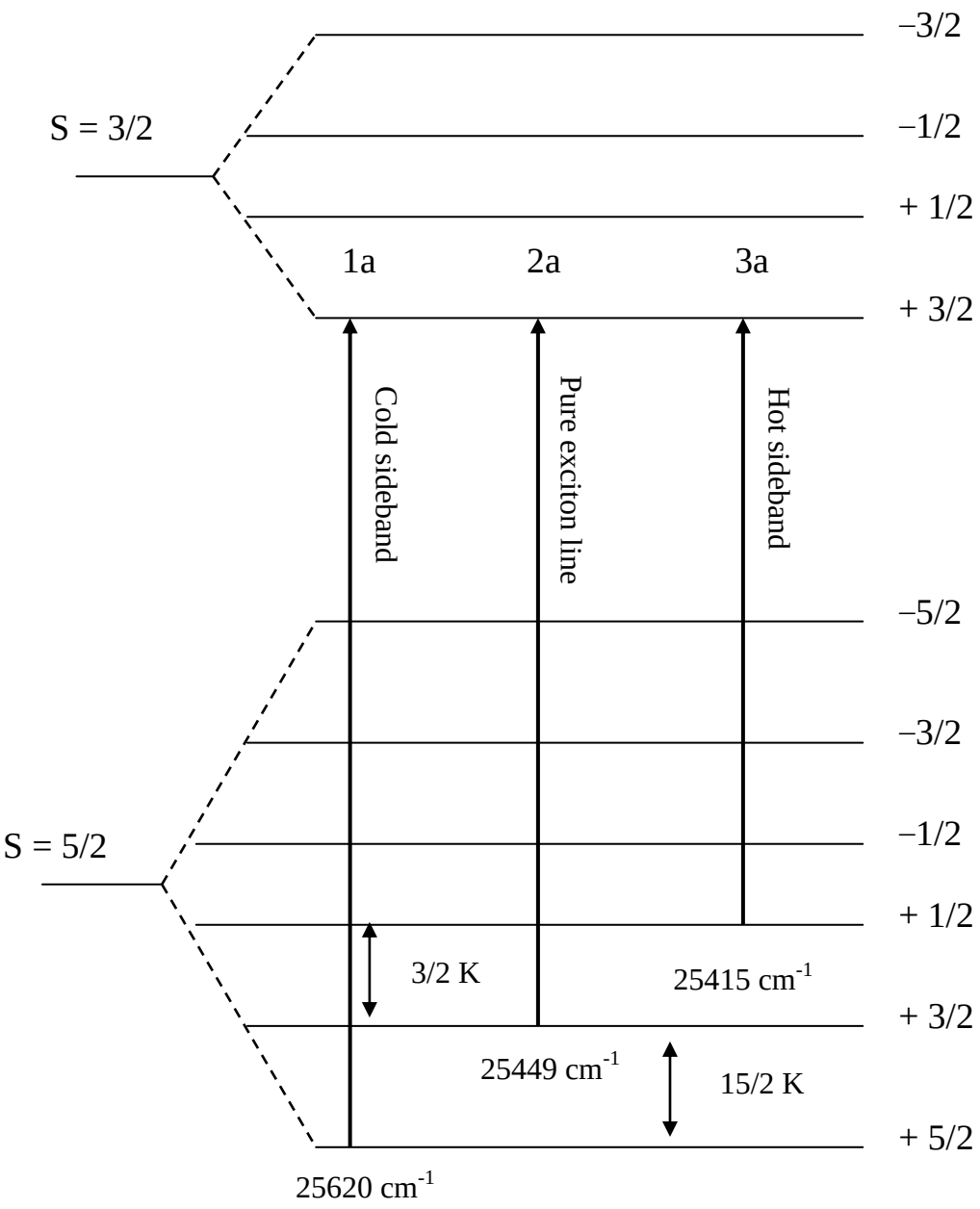

Figure 4.4: The energy values of exciton line, cold and hot sidebands for the first group.

Table 4.3: The summary of the experimental and theoretical results.

Energy transitions	Theoretical energy	Observed energy	Band type
(1a, 4)	$E_o + \Delta e_{11} - \Delta e_{21} + \Delta e_s$	25620 cm^{-1}	Cold sideband
(2a)	$E_o + \Delta e_{12} - \Delta e_{21}$	25449 cm^{-1}	Pure exciton line
(3a, 5)	$E_o + \Delta e_{13} - \Delta e_{21} - \Delta e_s$	25415 cm^{-1}	Hot sideband
(1b, 4)	$E_o + \Delta e_{12} - \Delta e_{22} + \Delta e_s$	25914 cm^{-1}	Cold sideband
(2b)	$E_o + \Delta e_{13} - \Delta e_{22}$	25773 cm^{-1}	Pure exciton line
(3b, 5)	$E_o - \Delta e_{13} - \Delta e_{22} - \Delta e_s$	25726 cm^{-1}	Hot sideband
(1c, 4)	$E_o - \Delta e_{13} + \Delta e_{21} + \Delta e_s$	25405 cm^{-1}	Cold sideband
(2c)	$E_o - \Delta e_{12} + \Delta e_{21}$	25338 cm^{-1}	Pure exciton line
(3c, 5)	$E_o - \Delta e_{11} + \Delta e_{21} - \Delta e_s$	25315 cm^{-1}	Hot sideband
(1d, 4)	$E_o + \Delta e_{13} + \Delta e_{22} + \Delta e_s$	25570 cm^{-1}	Cold sideband
(2d)	$E_o - \Delta e_{13} + \Delta e_{22}$	25561 cm^{-1}	Pure exciton line
(3d, 5)	$E_o - \Delta e_{12} + \Delta e_{22} - \Delta e_s$	25515 cm^{-1}	Hot sideband

Chapter Five

Summary

The study of the optical spectra in different manganese compounds and the details of its fine structure show the role of magnetic interactions and provide a clear picture of the energy structure of the antiferromagnetic phase in an organic complex of transition elements. The optical absorption spectra of high-spin $3d^5$ manganese ion in MnF_2 crystal (T_N = 67.3 K) has been studied. Several absorption bands have been observed and attributed to d^5-d^5 transitions, and their fine structures appear in the antiferromagnetic phase.

The d^5-d^5 transitions are both parity and spin forbidden for the electric dipole operator. There are four possible mechanisms which may break the parity and spin selection rules for electric dipole transitions: The first possible way is a single-ion mechanism, where the parity selection rule is overcome by vibronic interaction and the spin selection rule is overcome by spin-orbit interaction. The other mechanisms (B, C, and D) consist of the coupling between a pair of manganese ions. In mechanism B the parity selection rule is overcome by vibronic interaction and the spin selection rule by the exchange interaction. In mechanism C the parity selection rule is lifted by the exchange interaction and the spin selection rule by the spin-orbit interaction. In mechanism D the parity and spin selection rules are lifted by the exchange interaction.

The investigation of fine structure of pure exciton-magnon bands in the frequency range of the C-band $^6A_{1g}$ (^6S) → $^4A_{1g}$, ^4E_g (^4G) yielded the following results:

1. At low temperature the most broad and intense bands become better resolved exhibiting several peaks associated with exciton-magnon transitions.

2. The exchange interaction produces important modifications into the spectra of divalent manganese in MnF_2 compounds.

3. Most manganese compounds with similar crystal structures have the same number of peaks for each band. This leads the conclusion that the exchange interaction between the neighboring Mn^{+2} ions has a dominant role in the absorption process, and mechanism D (full exchange interaction) is responsible for lifting spin and parity selection rules of the C-band.

4. There is no noticeable shift of the line position of the C-band in the paramagnetic region. This is consistent with the C-band being a pure exciton-magnon band. Thus the C-band is ideal for the study of the effect of magnetic ordering.

5. Our calculations of the energy separations between the spin states by using spin-spin coupling are approximately close to the energy separations between the peak lines from the experimental data. This indicates that the spin-spin coupling of a pair of Mn^{+2} ions is the main mechanism responsible for the fine structure of the C-band at low temperature.

6. The spectrum of the C-band consists of four peaks, which are dominant at different temperature values contrary to the other peaks which lose intensity with increasing temperature. These four peaks are labeled as exciton transitions and have a dominant effect on the total band.

7. The sidebands associated with the main exciton transitions result from a pair ion interaction. The cold sideband involves creation of a magnon and refers to the higher energy, and the hot sideband involves annihilation of a magnon and refers to the lower energy.

References

Abumansoor, S. (1985): **Antiferromagnetic Ordering Effect on the Optical Transitions in MnF_2.** Thesis, West Virginia University, USA.

Ballhausen, C. (1962): **Introduction to Ligand Field Theory**. McGraw-Hill, New York, SanFrancisco, Toronto, London.

Bethe, H. (1929): "Theory of Brillouin Zones and Symmetry Properties of Wave Functions in Crystals". Ann. Phys., **3**, 133.

Blatt, J. and Weisskopf, V. (1952): **Theoretical Nuclear physics**. John Wiley and Sons, USA.

Condon, E. and Shortley, G. (1957): **The Theory of Atomic Spectra**. Cambridge Univ. Press, London, New York.

Cotton, F. (1963): **Chemical Applications of Group Theory**. Interscince Publisher, New York.

Cotton, F. and Wilkinson, G. (1980): **Advanced Inorganic Chemistry, A Comprehensive Text.** Fourth Edition, John Wiley and Sons, Inc.

Darwish, S., Abumansoor, S., and Seehra, M. (1986): "Thermal Behavior of the Two-Exciton Bands in MnF_2 and $RbMnF_3$". Phys. Rev. B, **34**, 147.

Darwish, S. and Seehra, M. (1988): "Vibronically Induced Two-Exciton Bands in $KMnF_3$ and $RbMnF_3$". Phys. Rev. B, **37**, 152.

Eisberg, R. and Resnick, R. (1974): **Quantum Physics of Atomic, Molecules, Solids, Nuclei and Particles.** John Wiley and Sons, Inc.

Eremenko, V. (1977): "Light Absorption in Antiferromagets". Advances in physics, **26**, 31.

Eremenko, V. and Shapiro, V. (1990): "Optical Spectroscopy of Antiferromagets with Different Structure Dimensionalities". Fizika Nizkikh Temperature, **12**, 1499.

Eremenko, V., Kachur, I., Piryatinskaya, V., and Shapiro, V. (1994): "Low Temperature Exciton-Magnon Light Absorption in 2-d AFM NH_3 $(CH_2)_2$ NH_3MnCl_4". Physica B, **194**, 194.

Eremenko, V., Karachevtsev, V., Kazachkov, A., Shapiro, V., and Slavin, V. (1993): "Unusual Behavior of the Luminescence in Quasi-One-Dimensional Antiferromagnetic Crystal $CsMnCl_32H_2O$ at Low Temperature". Solid State Communication, **87**, 1027.

Erickson, R. (1953): "Neutron Diffraction Studies of Antiferromagnetism in Manganese Fluoride and Some Isomorphous Compounds". Phys. Rev., **90**, 779.

Eyring, H. Walter, J., and Kimble, G. (1944): **Quantum Chemistry**. John Wiley and Sons, Inc., New York.

Ferguson, J. (1968): "Electronic Absorption Spectra of $KMnF_3$, $RbMnF_3$, and MnF_2". J. Chem., **21**, 307.

Ferguson, J., Guggenheim, H. and Tanabe, Y. (1966): "The Effect of Exchange Interactions in the Spectra of Octahedral Manganese II Compounds". J. Phys. Soc. Japan, **21**, 692.

Figgis, B. (1966): **Introduction to Ligand Fields**. Introduction Publisher, New York, London, Sudney.

Figgis, B. and Hitchman, M. (2000): **Ligand Field Theory and Its Application**. John Wiley and Sons.

Fujiwara, T. and Tanabe, Y. (1972):"Temperature Dependence of Magnon Sideband". J. Phys. Soc. Japan, **32**, 912.

Fujiwara, T., Gebhardt, W., Petanides, K., and Tanabe, Y. (1972):"Temperature Dependent Oscillator Strengths of Optical Absorptions in MnF_2 and $RbMnF_3$". J. Phys. Soc. Japan, **33**, 39.

Goode, D. (1965): "Optical Absorption Spectrum of Mn^{+2} in Cubic and Tetragonal Ligand Fields". J. Chem. Phys., **43**, 2830.

Greene, R., Sell, D., and White, R. (1967): "Exciton-Magnon Effects in the Optical Spectrum of MnF_2". Phys. Rev., **158**, 489.

Greene, R., Sell, D., Yen, W., and Schawlow, A. (1965): "Observation of A Spin-Wave Sideband in the Optical Spectrum of MnF_2**,** Phys. Rev. Lett., **15**, 656.

Griffel, M. and Stout, J. (1950): "Preparation of Single Crystals of Manganous Fluoride. The Crystal Structure from X-Ray Diffraction. The Melting Point and Density". J. Am. Chem. Soc., **72**, 4351-4353.

Griffith, J. (1961): **The Theory of Transition-Metal Ions**. Cambridge Univ. Press.

Griffiths, D. (1995): **Introduction to quantum mechanics**. Englewood Oliffs, New Jersey.

Gurylev, V., Vereshchagin, V., Dimitriev, I, and Kurbatov, L. (1975): Phys. Stat. Sol. (b), **69**, 639.

Harada, I. and Motizuki, K. (1972): "Effect of Magnon-Magnon Interaction on Spin Wave Dispersion and Magnon Sideband in MnS". J. Phys. Soc. Japan, **32**, 927.

Heller, P. and Benedek, G. (1962):"Nuclear Magnetic Resonance in MnF_2 near the Critical Point". Rev. Lett., **8**, 428.

Henderson, B. and Bartram, R. (2000): **Crystal Field Engineering of Solid-State Laser Material.** Cambridge University Press.

Hersberg, G. (1945): **Infrared and Ramman Spectra.** D. Van Nostrand Co., Inc., New York.

Hoekstra, H., Boudwijn, P, Groenier, H. and Haas, C. (1983): "Optical Absorption and Magnetic Circular Dichroism of MnI_2", Physica B, **121**, 62.

Hoekstra, H. and Haas, C. (1985): "Optical Absorption and Magnetic Circular Dichroism of $MnCl_2$", Physica B, **128**, 327.

Hoekstra, H., Folkersma, H., and Haas, C. (1985): "Optical Absorption and Magnetic Circular Dichroism of $MnBr_2$", Physica B, **128**, 133.

Huheey, J., Keiter, E., and Keiter, R. (1993): **Inorganic Chemistry: Principles of Structure and Reactivity**, Fourth Edition. Harper Collins Collage.

Jackson, J (1998): **Classical Electrodynamics.** Third Edition, John Wiley and Sons, Inc. New York, Chichester, Weinheim, Brisbane, Singapore, Toronto.

Kittel, C. (1996): **Introduction to Solid State Physics**, Seventh Edition. John Wiely Sons, Inc., New York..

Koide, S., and Pryce, M. (1958): "Infrared Absorption Spectra of Aquo Complexes and the nature of co-ordination Bonds". Phil. Mag., **3**, 607.

Laporte, O. (1942):"Term Formulae for the Configuration d^5". Phys. Rev., **61**, 302.

Lawson, K. (1966): "Optical Absorption Spectrum of Mn^{+2}, Fe^{+2}, and Co^{+2} in Dihydrated Halide Crystals". J. Chem. Phys., **44**, 4159.

Levine, I. (1983): **Quantum Chemistry,** Third Edition. Allyn and Bacon Inc. Boston, London, Sydney, Toronto.

Liboff, R. (1992): **Introductory Quantum Mechanics.** Addison-Wesley Pub Co.

Liehr, A. and Ballhausen, C. (1957): "Intensities in Inorganic Complexes". Phys. Rev., **106**, 1161.

Lockwood, D. and Cottam, M. (1988): "The Spin-Phonon Interaction in FeF_2 and Mnf_2 Studied by Raman Spectroscopy". J. App. Phys., **64**, 5876.

Lockwood, D., Katiyar, R., and V. C. Y. So (1983): "B_{1g} Mode Softening in FeF_2". Phys. Rev. B, **28**, 1983.

Low, W. (1960): **Paramagnetic Resonance in Solids**. Academic Press, New York.

Löwdin, P. (1962):"Exchange, Correlation, and Spin Effects in Molecular and Solid-State Theory". Rev. Mod. Phys., **34**, 80.

Macfarlane, R., Allen, J. (1971):"Exciton Bands in Antiferromagnetic Cr_2O_3". Phys. Rev.B, **4**, 3054.

Malakhovskii, A. and Vasilev, G. (1983):"The Origin of Anomalous Temperature Dependencies of Intensities of Spin-Forbidden d-d Transitions in Octahedral Complexes". Solid State Commun., **48**, 353.

Malakhovskii, A., Filimonov, V., and Goncharov, E. (1989): "Exciton-Magnon Absorption of Light in $MnCO_3$ above the Neel Temperature". Phys. Lett. A, **138**, 412.

Malakhovskii, A., Vasilev, G., and Morozova, T. (1986): "Temperature Dependences of $^6A_{1g} \rightarrow {}^4A_{1g}$, ^4E_g (^4G) and $^6A_{1g} \rightarrow {}^4E_g$ (^4D) Absorption Bands in $RbMnF_3$ in Paramagnetic State". Phys. Stat. Sol.(b), **138**, 285.

Majumdar, S. (1995): **Quantum Mechanics**. Delhi-32, New Delhi, Mombay, Madras, Calutta, Patna, Kanpur.

Moncorge, R. and Jacquier, B. (1981): "Pure Exciton and Magnon Sideband Optical Transitions in $BaMnF_4$". Phys. Lett., **85**, P. 390.

Moriya, T. and Inoue, M. (1968):"Effects of Spin Waves on Spin-Allowed Optical Transitions". J. Phys. Soc. Japan, **24**, P. 1251.

Motizuki, K and Harada, I. (1970): "Temperature Dependance of the Intensity of Magnon Sidebands in Cubic Antiferromagnetic Manganese Compound". Progr. Theor. Phys. Supp., **46**, 40.

Okazaki, A., Tuberfield, C., and Stevenson, R. (1964): "Longitudinal spin fluctuations in the antiferromagnet MnF_2 studied by polarized neutron scattering". Phys. Lett., **8**, 9.

Orgel, L. (1953):"Spectra of Transition-Metal Complexes". J. Chem. Phys., **23**, 1004.

Popov, E. (2003): "Optical Investigation of the Phase State of A Dilute Antiferromagnetic". Russian Physics J., **46**, 1253.

Popov, E. and Edelman, I. (2003): "Optical Absorption of the Diluted 2-d Antiferromagnet Rb_2MnCl_4". J. of Magnetism and Magnetic Materials, **258**, P. 134.

Popov, E, and Ovchinnikov, S. (2003): "Magnon Satellite Bands in the Optical Spectrum of Antiferromagnetic Rb_2MnCl_4", Phys. Of the Solid State, **45**, 1500.

Powell, L. and Crasemann, B. (1961): **Quantum Mechanics**. Addison-Wesley Pub (Sd).

Racah, G. (1942):"Theory of Complex Spectra II". Phys. Rev., **62**, 438.

Saito, F. (1970): "Exciton, magnon and phonon structures of the absorption spectra of $CsMnF_3$ in the 3900 Å region". Solid State Communications, **8**, 969.

Schwartz, R., Spencer, J., Yeakel, W., Schatz, P., and Maisch, W. (1974): "Magnetic circular dichroism of the $^4A_1$, ^4E region in the antiferromagnetic MnF_2 and K_2MnF_4". J. Chem. Phys.**, 60**, 2598.

Seehra, M. and Abumansoor, S. (1985): "Effect of Antiferromagnetic Ordering on the Optical Transition in MnF_2". Solid State Communications, **56**, 97.

Sell, D. (1968):"Review of Magnon-Sideband Experiment". J. App. Phys., **29**, 1030.

Sell, D., Greene, R, and White, R. (1967):"Optical Exciton-Magnon Absorption in MnF_2". Phys. Rev., **158**, P.498.

Sherman, D. (1984): "The Electronic Structures of Manganese Oxide Minerals". American Mineralogist, **69**, 788.

Shinagawa, K. and Tanabe, Y. (1971):"Intensity of Magnon Sideband". J. Phys. Soc. Japan, **30**, 1280.

Slater, J. (1960): **Quantum Theory of Atomic Structure**, Vol. 1. McGraw-Hill, New York, Toronto, London.

Slater, J. (1974): **The Self-Consistent Field for Molecules and Solids: Quantum Theory of Molecules and Solids**. McGraw-Hill, New York, London, Sydney.

Suzuki, N. and Kamimura, H. (1973): "Theory of Spin-Dependent Phonon Raman Scattering in Magnetic Crystal". J. Phys. Soc. Japan, **35**, 985.

Sugano, S., Tanabe, Y., and Kamimura, H. (1970): **Multiplets of Transition-Metal Ions in Crystals**. Academic Press, New York, London. 62.

Tanabe, Y, and Gondaira, K. (1967):"Spin Wavebands in MnF_2". J. Phys. Soc., **22**, 573.

Tanabe, Y. and Sugano, S. (1954):"On the Optical Absorption Spectra of Complex Ions I". J. Phys. Soc. Japan, **9**, 753.

Tanaka, H. (1971): "Thermal Behavior of Magnon Side-Bands in Antiferromagets". J. Phys. Soc. Japan, **31**, 368.

Tinkham, M. (1964): **Group Theory and Quantum Mechanics**. McGraw-Hill, New York.

Trapp, C. and Stout, J. (1963):"Magnetic Susceptiplity of MnF_2". Phys. Rev. Lett., **10**, 157.

Tsuboi, T. and Ahmet, P. (1992): "Temperature Dependence of the Optical Exciton-Magnon Absorption lines in MnF_2". Phys. Rev. B, **45**, 468.

Tsuboi, T. and Kleemann, W. (1983): "Exciton and Magnon-Sideband Absorption in the Pyroelectric Antiferromagnet $BaMnF_4$". Phys. Rev. B, **27**, 3762.

Tsujikawa, I. and Kanda, E. (1963)**: "Spectroscopic Studies of the Ordered State of the Manganous Halide Tetrahydrates".** J. Phys. Soc. Japan**,** 18**,** 1382.

Van Vleck, J. (1932): **Electric and Magnetic Susceptibilities.** Oxford University Press, Oxford and New York.

Van Vleck, J. (1939): "The Jahn-Teller Effect and Crystalline Stark Splitting for Clusters of the Form XY_6". J. Chem. Phys., **7**, 72.

Wong, Y., Scarpace, F., Pfeifer, C., and Yen, W. (1974): "Circular and Magnetic Circular Dichroism of Some Simple Antiferromagnetic Fluorides". Phys. Rev. E, **9**, 3086.

Wychoff, R. (1948): **Crystal Structure**, Vol. 1. Interscince, New York.

Yen, W., Imbusch, G., and Huber, D. (1967): **In Optical Properties of Ions in Crystals**, edited by H. Grosswhite and H. Moos, Interscince, New york..

Yen, W. and Selzer, P. (1981): **Laser Spectroscopy of Solids**. Berlin Heidelberg, New York.

Yokogawa, M., Taniguchi, K., and Hamaguchi, C. (1977): "Fine Structure in Optical Spectra of MnO". J. Phys. Soc. Japan, **42**, 591.

Zabluda, V., Malakhovskii, A., and Edelman, I. (1985): Fiz. Tverd. Tela., **27**, 133.

Appendices

Appendix A

The real Parts of d-orbitals:

The imaginary forms of the five d-orbitals are generated from the following spherical harmonic (Griffiths, 1995):

$$Y_2^{\ 0} = (5/8)^{1/2} \left(3\cos^2\theta - 1\right).(2\pi)^{-1/2} \quad \text{A.1}$$

$$Y_2^{\ \pm 1} = (15/4)^{1/2} \sin\theta\cos\theta.(2\pi)^{-1/2} e^{\pm i\phi} \quad \text{A.2}$$

$$Y_2^{\ \pm 2} = (15/16)^{1/2} \sin^2\theta\,.(2\pi)^{-1/2} e^{\pm 2i\phi} \quad \text{A.3}$$

By a combination of the imaginary forms of the orbitals to produce the real forms that do not contain i and affected by crystal field, we note that (Figgis, 1966):

$$e^{\pm im\phi} = \cos(m\phi) \pm i\sin(m\phi) \quad \text{A.4}$$

Where m is the same as m_l

$$x = r\sin\theta\cos\phi \qquad y = r\sin\theta\sin\phi \qquad z = r\cos\theta \quad \text{A.5}$$

Let us use calculated the combination:

$$[(+1) + (-1)] \quad \text{A.6}$$

Where +1 and -1 means the wave functions corresponding to m = +1 and -1 respectively.

$$(+1) = R_{n,2}\, Y_2^{+1} \qquad (-1) = R_{n,2}\, Y_2^{-1} \quad \text{A.7}$$

$$Y_l^m(\theta,\phi) = (2\pi)^{-1/2}\, \Theta_{lm}(\theta) e^{im\phi} \quad \text{A.8}$$

$$\Theta_{2,\pm 1} = \mp\sqrt{\frac{15}{4}} \sin\theta\cos\theta \quad \text{A.9}$$

By substituting these values, A.6 becomes:

$$(+1) + (-1) = 2R_{n,2}\sqrt{\frac{15}{4}}(2\pi)^{-1/2} \sin\theta\cos\theta\cos\phi = 2R_{n,2}\sqrt{\frac{15}{4}}(2\pi)^{-1/2}\frac{xz}{r^2} \approx xz \quad \text{A.10}$$

In the last step all the factors other than function of the Cartesian coordinates are omitted.

The new wave function (Ψ) in the last equation must be normalized as the following:

$$\frac{\Psi}{\left(\int \Psi^{*}\Psi\, d\tau\right)^{1/2}} \qquad \text{A.11}$$

$$\int_{0}^{2\pi} \Phi^{*}\Phi\, d\Phi = \begin{cases} 1 & if\ \ m = m' \\ 0 & if\ \ m \neq m' \end{cases} \qquad \text{A.12}$$

Now

$$\int_{0}^{2\pi} \left[(+1)+(-1)\right]^{*}\left[(+1)+(-1)\right] d\tau = \int_{0}^{2\pi} (1)^{*}(1)+(1)^{*}(-1)+(-1)^{*}(1)+(-1)^{*}(-1)\, d\tau$$

$$= 1+0+0+1 = 2 \qquad \text{A.13}$$

$$d_{xz} = \left[(1)+(-1)\right] \Big/ \left(\int \left[(1)+(-1)\right]^{*}\left[(1)+(-1)\right] d\tau\right)^{1/2} = \ (2)^{-1/2}\left[(1)+(-1)\right] \qquad \text{A.14}$$

By making other suitable combinations of the imaginary parts of d-orbitals we can obtain the following results:

$$\begin{aligned} d_{z^2} &= (0) \\ d_{xy} &= 2^{-1/2}\left[(2)-(-2)\right] \\ d_{yz} &= 2^{-1/2}\left[(1)-(-1)\right] \\ d_{x^2-y^2} &= 2^{-1/2}\left[(2)+(-2)\right] \end{aligned} \qquad \text{A.15}$$

Appendix B

Slater-Condon parameters

F_K's are abbreviation of the Slater integral F^K's (dd) which is given by:

$$F^K(dd) = \int_0^\infty r_1^2\, dr_1 \int_0^\infty r_2^2\, dr_2\, R_d^2(r_1) R_d^2(r_2)\, r_<^K / r_>^{K+1} \qquad \text{B.1}$$

Where $r_<$ is the lesser and $r_>$ is the larger of r_1 and r_2.
The F_K's are given in terms of F^K's as:

$F_0 = F^0$, $F_2 = 1/49\ F^2$, $F_4 = 1/144\ F^4$. B.2

Appendix C

Crystal potential field:

Consider the central ion surrounded by six negative point-charges (Ze) with distance a as shown in figure C.1. The potential energy V_c of an electron of the central ion due to the field of the point-charges is given by Sugano, Tanabe, and Kamimura (1970):

$$V_c(r) = \sum_{j=1}^{6} \frac{Ze^2}{r_j - r} \qquad \text{C.1}$$

r_j is the position vector of the j^{th} point charge, and r is the electron coordinate. $1/r_j$-r can be expanded in spherical harmonics as follows: (Eyring, Walter, and Kimball, 1944)

$$\frac{1}{r_j - r} = \sum_{l=0}^{\infty} \sum_{m=-l}^{l} \frac{4\pi}{2l+1} \cdot \frac{r_<^l}{r_>^{l+1}} Y_l^m(\theta,\phi) Y_l^{m^*}(\theta_j,\phi_j) \qquad \text{C.2}$$

Where $r_<$ is the lesser and $r_>$ the greater of a and r. (r, θ, Φ) and (r_j, θ_j, Φ_j) are the spherical coordinates of r and r_j respectively. When a is much larger than the radius of the central ion r, then $r_>$ and $r_<$ respectively are replaced by a and r. C.1 for the six point charges becomes:

$$V_c(r) = 6Ze^2 \sum_{l=0}^{\infty} \sum_{m=-l}^{l} \frac{4\pi}{2l+1} \frac{r^l}{a^{l+1}} Y_l^m(\theta,\phi) Y_l^{m^*}(\theta_j,\phi_j) \qquad \text{C.3}$$

The spherical harmonic $Y_l^m(\theta,\phi) = (2\pi)^{-1/2} \Theta_{lm}(\theta) e^{im\phi}$

Suppose:

$$Q_{lm} = \left(\frac{4\pi}{2l+1}\right)^{1/2} \frac{6Ze^2}{a^{l+1}} Y_l^{m^*}(\theta_j,\phi_j) \qquad \text{C.4}$$

$$C_l^m(\theta_i \phi_i) = \left(\frac{4\pi}{2l+1}\right)^{1/2} Y_l^m(\theta,\phi) \qquad \text{C.5}$$

C.3 can be written as:

$$V_c(r) = \sum\sum r^l \, Q_{lm}(\theta_j,\phi_j) C_l^m(\theta,\phi) \qquad \text{C.6}$$

Since $(\theta \;\; \phi), (\theta_j \;\; \phi_j)$ are known to be $\left(\frac{\pi}{2} \;\; 0\right), \left(\frac{\pi}{2} \;\; \frac{\pi}{2}\right), \ldots$

Then Q_{lm}'s are given:

When m = 0

$$Q_{l0} = \left(\frac{2}{2l+1}\right)^{1/2} \frac{6Ze^2}{a^{l+1}} \left[\Theta_{l0}(0) + 4\Theta_{l0}\left(\frac{\pi}{2}\right) + \Theta_{l0}(\pi)\right] \qquad \text{C.7.a}$$

When m is even

$$Q_{lm} = \left(\frac{2}{2l+1}\right)^{1/2} \frac{6Ze^2}{a^{l+1}} \Theta_{lm}\left(\frac{\pi}{2}\right)\left[1 + e^{im\frac{\pi}{2}} + e^{im\pi} + e^{im\frac{3\pi}{2}}\right] \qquad \text{C.7.b}$$

When m is odd

$$Q_{lm} = 0 \qquad \text{C.7.c}$$

By inserting the forms of $\Theta_{lm}(\theta)$ are given in table C.1 into C.7a-c, then V_c can be written as:

$$V_c(r) = \frac{6Ze^2}{a} + \frac{7Ze^2}{2a^5} r^4 \left\{C_4^0(\theta_i\phi_i) + \left(\frac{5}{14}\right)^{1/2}\left[C_4^4(\theta_i\phi_i) + C_4^{-4}(\theta_i\phi_i)\right]\right\}$$
$$+ \frac{3Ze^2}{4a^7} r^6 \left\{C_6^0 - \left(\frac{7}{2}\right)^{1/2}\left[C_6^4 + C_6^{-4}\right]\right\} + \ldots \qquad \text{C.8}$$

All of the terms with $l > 4$ will vanish because they are very small and approach zero. Substitute the C's value in C.9:

$$V_c(r) = \frac{6Ze^2}{a} + \frac{7Ze^2\sqrt{\pi}}{3a^5} r^4 \left[Y_4^0 + \sqrt{\frac{15}{4}}\left(Y_4^4 + Y_4^{-4}\right)\right] \qquad \text{C.9}$$

Where:

$$Y_4^0 = \sqrt{\frac{9}{4\pi}}\sqrt{\frac{1}{64}}\frac{35z^4 - 30z^2r^2 + 3r^4}{r^4} \qquad \text{C.10.a}$$

$$Y_4^4 = \sqrt{\frac{9}{4\pi}}\sqrt{\frac{35}{128}}\frac{(x+iy)^4}{r^4} \qquad \text{C.10.b}$$

$$Y_4^{-4} = \sqrt{\frac{9}{4\pi}}\sqrt{\frac{35}{128}}\frac{(x-iy)^4}{r^4} \qquad \text{C.10.c}$$

From 11a….c, equation 10 is given as:

$$V_c(r) = \frac{6Ze^2}{a} + \frac{35Ze^2}{4a^5}\left(x^4 + y^4 + z^4 - \frac{3}{5}r^4\right) \qquad \text{C.11}$$

$$D = \frac{35Ze^2}{4a^5}$$

$$q = \left(\frac{2}{105}\right)\int_0^\infty R_{nl}^*(r)\, r^4\, R_{nl}(r) r^2\, dr$$

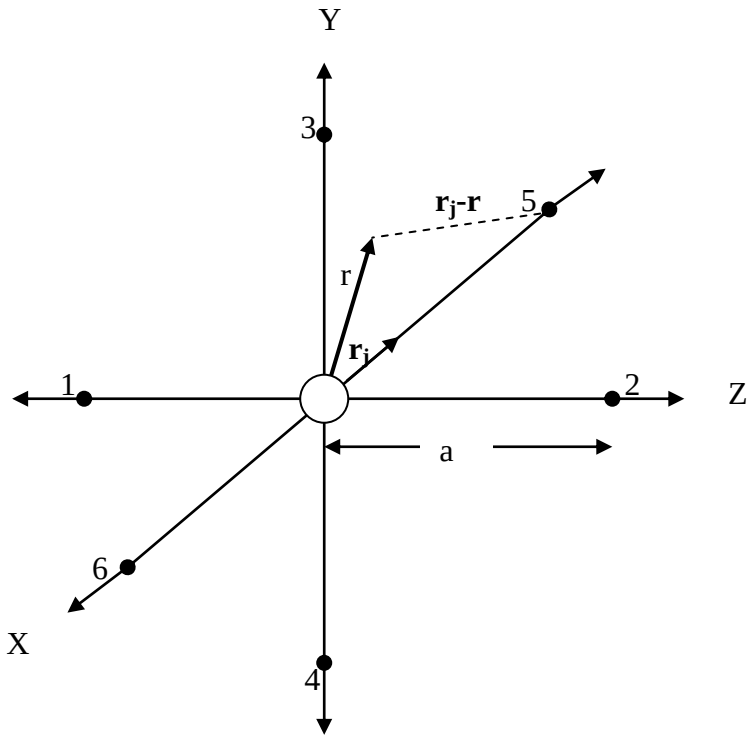

Figure C.1: The polar coordinates of an electron of the central ion in the field of negative charges

Table C.1: Explicit Forms of $\Theta_{lm}(\theta)$ (Sugano, Tanabe, and Kamimura, 1970).

$$\Theta_{lm}(\theta) = (-1)^m \left(\frac{(2l+1)(l-m)}{2(l+m)} \right)^{1/2} \sin^m \theta \frac{d^m}{(d\cos\theta)^m} P_l(\cos\theta),$$

$$\Theta_{l-m}(\theta) = (-1)^m \Theta_{lm}(\theta), \qquad m \geq 0.$$

Θ_{00}	$1/\sqrt{2}$
Θ_{10}	$\left(\sqrt{3}/\sqrt{2}\right)\cos\theta$
$\Theta_{1\pm1}$	$\mp\left(\sqrt{3}/2\right)\sin\theta$
Θ_{20}	$\left(\sqrt{5}/2\sqrt{2}\right)\left(2\cos^2\theta - \sin^2\theta\right)$
$\Theta_{2\pm1}$	$\mp\left(\sqrt{15}/2\right)\cos\theta\sin\theta$
$\Theta_{2\pm2}$	$\left(\sqrt{15}/4\right)\sin^2\theta$
Θ_{30}	$\left(\sqrt{7}/2\sqrt{2}\right)\left(2\cos^3\theta - 3\cos\theta\,\sin^2\theta\right)$
$\Theta_{3\pm1}$	$\mp\left(\sqrt{21}/4\sqrt{2}\right)\sin\theta\,\left(4\cos^2\theta - \sin^2\theta\right)$
$\Theta_{3\pm2}$	$\left(\sqrt{105}/4\right)\cos\theta\sin^2\theta$
$\Theta_{3\pm3}$	$\mp\left(\sqrt{35}/4\sqrt{2}\right)\sin^3\theta$
Θ_{40}	$\left(3/8\sqrt{2}\right)\left(8\cos^4\theta - 24\cos^2\theta\,\sin^2\theta + 3\sin^4\theta\right)$
$\Theta_{4\pm1}$	$\mp\left(3\sqrt{5}/4\sqrt{2}\right)\cos\theta\sin\theta\left(4\cos^2\theta - 3\,\sin^2\theta\right)$
$\Theta_{4\pm2}$	$\left(3\sqrt{5}/8\sqrt{2}\right)\sin^2\theta\left(6\cos^2\theta - \sin^2\theta\right)$
$\Theta_{4\pm3}$	$\mp\left(3\sqrt{35}/4\sqrt{2}\right)\cos\theta\sin^3\theta$
$\Theta_{4\mp4}$	$\left(3\sqrt{35}/16\right)\sin^4\theta$

Appendix D

The effect of octahedral field on d-orbitals:

To illustrate the effect of octahedral field on d-orbitals, consider crystal potential V_c that resulted from appendix C equation 9:

$$V_c(r) = \frac{6Ze^2}{a} + \frac{7Ze^2\sqrt{\pi}}{3a^5}\, r^4 \left[Y_4^0 + \sqrt{\frac{15}{4}} \left(Y_4^4 + Y_4^{-4} \right) \right] \qquad \text{D.1}$$

The first term is spherically symmetrical:

$V_{oct} = V_c(r) - 6Ze^2/a$ D.2

By applying the matrix element of V_{oct} on the orbital parts of the wave functions by using the following equation:

$$\langle m | V_{oct} | m' \rangle = \langle R_{nl}\, Y_l^m \, | V_{oct} | \, R_{n'l'}\, Y_{l'}^{m'} \rangle \qquad \text{D.3a}$$

$$\frac{7Ze^2}{3a^5} \sqrt{\pi}\, \langle R_{nl} \left| r^4 \right| R_{n'l'} \rangle \left[\langle Y_l^m \left| Y_4^0 \right| Y_{l'}^{m'} \rangle + \sqrt{\frac{5}{14}} \left(\langle Y_l^m \left| Y_4^4 \right| Y_{l'}^{m'} \rangle \, \langle Y_l^m \left| Y_4^{-4} \right| Y_{l'}^{m'} \rangle \right) \right] \qquad \text{D.3b}$$

Note that:

$\int_0^{2\pi} Y_{l_1}^{m_1}\, Y_{l_2}^{m_2}\, Y_{l_3}^{m_3}\, d\phi \neq 0$ Only when the following conditions are satisfied:

$$l_1 + l_2 + l_3 = even \quad and \quad m_2 = m_1 - m_3 \qquad \text{D.4}$$

In our case for d-wave functions:

$$l_1 = l_3 = 2 \quad and \quad m_1 = m_3 = \pm 2, \pm 1, 0 \qquad \text{D.5}$$

When $m_1 = m_2 = 2$, then the matrices that involve Y_4^4 and Y_4^{-4} are zero and the matrix element $\langle Y_2^2 \left| Y_4^0 \right| Y_2^2 \rangle$ does not vanish. To evaluate this matrix let us define a quantity:

$$a^k(lm'', l'm') = \left(\frac{4\pi}{2k+1} \right)^{1/2} \langle Y_l^{m''} \left| Y_k^m \right| Y_{l'}^{m'} \rangle \qquad \text{D.6}$$

From the values of a^k are given in table D.1 for s, p, and d electrons, when k = 4 and m'' = m' = 2 then:

$$\langle Y_2^2 \left| Y_4^m \right| Y_2^2 \rangle = \sqrt{\frac{9}{4\pi}} \sqrt{\frac{1}{441}} \qquad \text{D.7}$$

By substituting D.5 in D.3, the result is:

$$\frac{7Ze^2}{3a^5}\sqrt{\pi}\sqrt{\frac{9}{4\pi}}\sqrt{\frac{1}{441}}\,\langle R_{nl}\left|r^4\right|R_{n'l'}\rangle=\frac{1}{6}\frac{Ze^2}{a^5}\langle R_{nl}\left|r^4\right|R_{n'l'}\rangle \qquad \text{D.8}$$

$$D=\frac{35ze^2}{4a^5} \qquad \text{And} \qquad q=\frac{2}{105}\langle r^4\rangle_{nl}=\frac{2}{105}\int_0^\infty r^4\left|R_{nl}(r)\right|^2 r^2\,dr$$

By applying the same technique on the other d-wave functions we obtain the following results:

$$\langle -2\left|\,V_{oct}\right|-2\rangle=\frac{Ze^2\overline{r^4}}{6a^5}=D_q$$

$$\langle \pm1\left|\,V_{oct}\right|\pm1\rangle=-4\left(\frac{Ze^2\overline{r^4}}{6a^5}\right)=-4D_q$$

$$\langle\ 0\ \left|\,V_{oct}\right|0\ \rangle=6\left(\frac{Ze^2\overline{r^4}}{6a^5}\right)=6D_q$$

$$\langle \pm2\left|\,V_{oct}\right|\mp2\rangle=5\left(\frac{Ze^2\overline{r^4}}{6a^5}\right)=5D_q$$

Table D.1: $a^k\left(lm'',l'm'\right)$ for s, p, d electrons (Slater, 1960).

	m''	m'	K				
			0	1	2	3	4
ss	0	0	1	0	0	0	0
sp	0	±1	0	$-\sqrt{1/3}$	0	0	0
	0	0	0	$\sqrt{1/3}$	0	0	0
pp	±1	±1	1	0	$-\sqrt{1/25}$	0	0
	±1	0	0	0	$\sqrt{3/25}$	0	0
	±1	∓1	0	0	$-\sqrt{6/25}$	0	0
	0	0	1	0	$\sqrt{4/25}$	0	0
sd	0	±2	0	0	$\sqrt{1/5}$	0	0
	0	±1	0	0	$-\sqrt{1/5}$	0	0
	0	0	0	0	$\sqrt{1/5}$	0	0
pd	±1	±2	0	$-\sqrt{6/15}$	0	$\sqrt{3/245}$	0
	±1	±1	0	$\sqrt{3/15}$	0	$-\sqrt{9/245}$	0
	±1	0	0	$-\sqrt{1/15}$	0	$\sqrt{18/245}$	0
	±1	∓1	0	0	0	$-\sqrt{30/245}$	0
	±1	∓2	0	0	0	$\sqrt{45/245}$	0
	0	±2	0	0	0	$\sqrt{15/245}$	0
	0	±1	0	$-\sqrt{3/15}$	0	$-\sqrt{24/245}$	0
	0	0	0	$\sqrt{4/15}$	0	$\sqrt{27/245}$	0
dd	±2	±2	1	0	$-\sqrt{4/49}$	0	$\sqrt{1/441}$
	±2	±1	0	0	$\sqrt{6/49}$	0	$-\sqrt{5/441}$
	±2	0	0	0	$-\sqrt{4/49}$	0	$\sqrt{15/441}$
	⋮	⋮	⋮	⋮	⋮	⋮	⋮
